BEHAVIOR OF BOLTED TENSION SPLICE CONNECTIONS IN STEEL LATTICE OVERHEAD TRANSMISSION LINE TOWERS

A MASTER'S THESIS

in

Civil Engineering

Atilim University

by

GOKMEN SEN

OCTOBER 2014

BEHAVIOR OF BOLTED TENSION SPLICE CONNECTIONS IN STEEL LATTICE OVERHEAD TRANSMISSION LINE TOWERS

A THESIS SUBMITTED TO

THE GRADUATE SCHOOL OF NATURAL AND APPLIED SCIENCES

OF

ATILIM UNIVERSITY

BY

GOKMEN SEN

IN PARTIAL FULFILLMENT OF THE REQUIREMENTS

FOR

THE DEGREE OF MASTER OF SCIENCE OF PHILOSOPHY

IN

THE DEPARTMENT OF CIVIL ENGINEERING

OCTOBER 2014

Approval of the Graduate School of Natural and Applied Sciences, Atilim University.

_____

Prof. Dr. K. Ibrahim Akman

Director

I certify that this thesis satisfies all the requirements as a thesis for the degree of Master of Science.

_____

Assoc. Prof. Dr. Tolga Akış

Head of Department

This is to certify that we have read the thesis "Behavior of Bolted Tension Splice Connections in Lattice Overhead Transmission Line Towers" submitted by Gökmen Şen and that in our opinion it is fully adequate, in scope and quality, as a thesis for the degree of Master of Science.

_____	_____
Assoc. Prof. Dr. Eray Baran	Assoc. Prof. Dr. Tolga Akış
Co-Supervisor	Supervisor

Examining Committee Members

Assoc. Prof. Dr. Tolga Akış	_____
Assoc. Prof. Dr. Eray Baran	_____
Assist. Prof Dr. Halit Cenan Mertol	_____
Assist. Prof Dr. Gökhan Tunç	_____
Dr. Cenk Tort	_____

Date: 16/10/2014

I declare and guarantee that all data, knowledge and information in this document has been obtained, processed and presented in accordance with academic rules and ethical conduct. Based on these rules and conduct, I have fully cited and referenced all material and results that are not original to this work.

Name, Last name: Gokmen SEN

Signature:

ABSTRACT

BEHAVIOR OF BOLTED TENSION SPLICE CONNECTIONS IN STEEL LATTICE OVERHEAD TRANSMISSION LINE TOWERS

Sen, Gokmen

M.S., Civil Engineering Department

Supervisor: Assoc. Prof. Dr. Tolga Akis

Co-Supervisor: Assoc. Prof. Dr. Eray Baran

October 2014, 74 pages

Behavior of bolted splice connections in steel lattice overhead transmission line towers under tensile loads was experimentally studied. Seven specimens with each of them having a different connection detail were tested. The main parameters used in the testing program were the number of bolts used in the connection, presence of connection reinforcement angles, and the number and geometry of filler plates used between the main members. Main aim of the study was to gain a better understanding of the load-flow mechanism in the connection. The specimens were observed to exhibit similar response, which includes an initial linear behavior followed by a yielding portion and a secondary linear portion that continues until net section fracture of the upper main member. The measured load capacities of specimens were compared to the predicted capacity corresponding to the net section fracture of the upper main member. The measured and predicted capacities were observed to agree acceptably well with each other. Based on the experimental results, the redundant members in the connection were identified and recommendations were provided in order to simplify the connection geometry by eliminating the redundant members.

Keywords: Lattice overhead transmission line tower, bolted connection, splice connection, tension member.

ÖZ

ÇELİK KAFES HAVAİ ELEKTRİK HATTI DİREKLERİNDEKİ CİVATALI BAĞLANTILARIN ÇEKİ YÜKÜ ALTINDAKİ DAVRANIŞLARI

Şen, Gökmen

Yüksek Lisans, İnşaat Mühendisliği Bölümü

Tez Yöneticisi: Doç. Dr. Tolga Akış

Ortak Tez Yöneticisi: Doç. Dr. Eray Baran

Ekim 2014, 74 sayfa

Bu çalışmada çelik kafes havai elektrik hattı direklerinde kullanılan civatalı bağlantıların çeki yükü altındaki davranışı deneysel olarak incelenmiştir. Bu amaçla, herbirinde farklı bağlantı detayı kullanılan toplam yedi adet numune üzerinde yükleme deneyleri yapılmıştır. Deneysel programda kullanılan temel parametreler bağlantıda kullanılan civata sayısı, bağlantı bölgesinde takviye köşebentlerinin bulunup bulunmaması ve ana elemanlar arasında bulunan dolgu plakalarının sayısı ve geometrisidir. Çalışmanın temel amacı bağlantı bölgesindeki yük aktarım mekanizmasının belirlenmesidir. Test edilen bütün numunelerin oldukça benzer davranışlar sergiledikleri görülmüştür. Numuneler genel olarak başlangıçta doğrusal bir davranış göstermiş, bunun arkasından malzemede akma gerçekleşmiş ve ikinci bir doğrusal kısmın ardından üst ana elemanda kopma meydana gelmiştir. Numunelerin ölçülen kapasiteleri ile üst ana elemanda kopma oluşmasına karşılık gelen hesaplanmış kapasiteleri arasında belirgin bir uyum olduğu görülmüştür. Numunelerin deneysel olarak belirlenmiş davranışları göz önüne alındığında bağlantı bölgesinde bulunan ve yük aktarım mekanizmasına katkıda bulunmayan elemanlar saptanmıştır. Bu elemanların bağlantıdan çıkarılması suretiyle, halen kullanılmakta olan bağlantı geometrisinin oldukça basitleştirilebileceği yönünde tavsiyelerde bulunulmuştur.

Anahtar kelimeler: Çelik kafes havai elektrik hattı direği, civatalı bağlantı, bindirme bağlantısı, çekme elemanı.

To My Parents and Wife

ACKNOWLEDGMENTS

I would like to express my sincere appreciation to my supervisor Assoc. Prof. Dr. Tolga Akis and my co-supervisor Assoc. Prof. Dr. Eray Baran for their support and insight throughout the study. It was a great honor for me to work with them.

I would like to thank my friends Burhan Duyar and Metin Kurtoglu for their help during the laboratory phase of the research.

I am thankful to Atilim University Structural Mechanics Laboratory staff Ali Sener Dursunoglu and Suayip Ozdemir for their valuable help.

Thanks also to my company “Miteng.Inc” for financial support.

I also would like to express my deepest thanks to my parents and wife for their endless love, faith and support.

TABLE OF CONTENTS

LIST OF FIGURES

LIST OF TABLES

LIST OF SYMBOLS AND ABBREVATIONS

ASCE	American Society of Civil Engineers
AISC	American Institute of Steel Construction
PLS	Power Line Systems
YON	Yielding on net section
FON	Fracture on net section
YOG	Yielding on gross section
A_b	Nominal unthreaded body area of bolt
A_e	Effective net area
A_g	Gross section area
A_{gv}	Gross area subject to shear
A_n	Net section area
A_{nt}	Net area subject to tension
A_{nv}	Net area subject to shear
A_{req}	Required area
F_{nv}	Shear stress for bolts
F_u	Ultimate strength
F_y	Yield strength
g	Bolt spacing perpendicular to the load direction
L	Length of member
Le	Edge distance to sheared edges
Le’	Edge distance to rolled edges
N_{bolt}	Number of bolts
P_n	Nominal axial strength
R_n	Nominal strength
s	Bolt spacing horizontal to the load direction
t	Thickness of member
U	Shear lag factor
σ_y	Yield stress
σ_u	Ultimate stress

CHAPTER 1

INTRODUCTION

1.1. GENERAL

Transmission line towers are structures that play an important role in energy transfer from one point to another. One of the main roles of these structures is to transfer the energy safely and effectively with safe height from ground. The structures commonly used on transmission lines are either lattice type or pole type towers. Lattice tower structures are usually composed of steel angle sections [1].

1.1.1. TYPES OF LOADING

This study was conducted to investigate the main member tension splice connection behavior of an actual overhead transmission tower. Typical geometry of a lattice type overhead transmission tower can be seen in Figure 1.1.

Loads used for structural design of typical overhead transmission line towers are as follows:

- Wind and ice loads
- Installation and repair loads
- Equipment and conductor loads
- Earthquake load
- Broken wire load

Structural analysis and design of the tower are done according to these loads. The design procedure is explained in more detail in the following section.

1.1.2. ANALYSIS AND DESIGN METHODS

Members of the transmission line towers are designed based on tension and compression stresses emerge on them. ASCE 10-97 and AISC 360-10 are the base specifications for design procedure. In this thesis, only tension cases are considered in the connection behavior. Tower design flow chart for tension cases can be seen in

Figure 1.2. Loads to be applied to the structure are determined based on several factors, such as the location and type of the tower. Finite element model of the tower is generated and the structural analysis is performed using a software called PLS-Tower. Afterwards, member forces are computed and then member and bolt sizes are chosen not only to satisfy the code requirements and resist the external forces but also to achieve an optimal design. In addition, special for the transmission towers, members have to resist man-load during the maintenance and repair period if the angle of member is smaller than 30 degree to the horizontal.

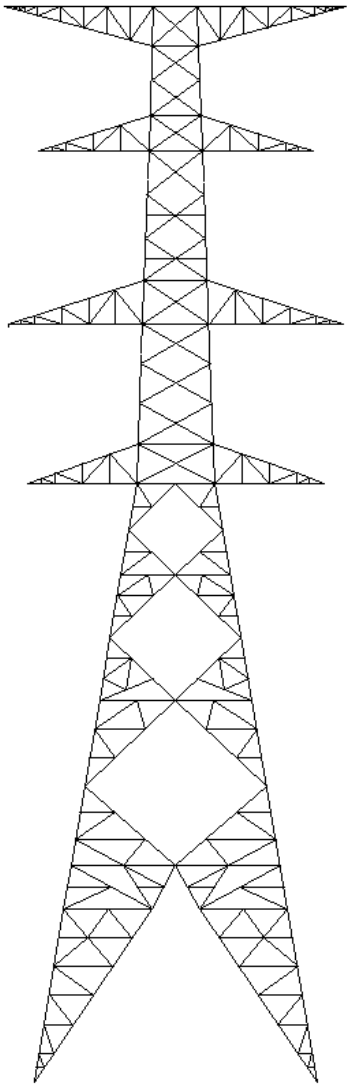

Figure 1.1. Overall geometry of a typical latticed tower

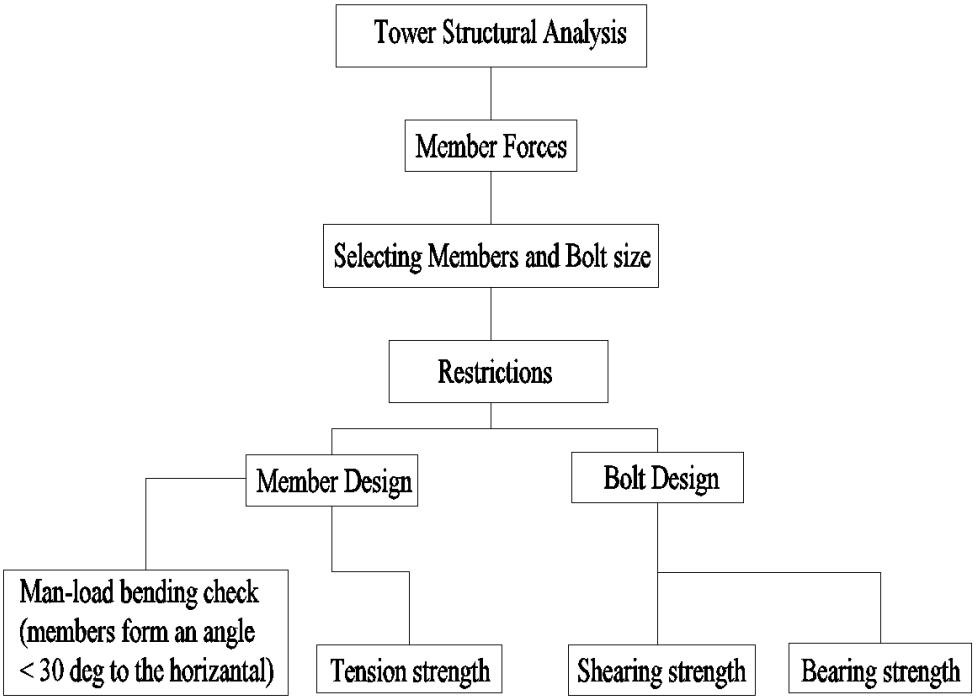

Figure 1.2. Tower design flow chart for tension

1.2. LITERATURE REVIEW

Barth, Orbison and Nukala [2] focused on examining the effects of connection eccentricity and connection length on the ultimate capacity of bolted tension members. The main objective of the work was to predict the failure capacities of tension members with medium to large connection eccentricities and varying connection lengths. For the experimental phase, sixteen WT 155x10.5 and six WT 100x18 specimens were tested. Apart from the experimental studies, the authors also conducted numerical analysis through finite element modelling (FEM). The numerical simulation results were reported to indicate an excellent agreement with the experimental failure capacities of the specimens with large connection eccentricities. In addition to this, the net section rupture failure mode of specimens was accurately captured through the numerical simulations. The results of this work ultimately led to proposed improved design equations for bolted connections subjected to direct tension.

Zhuge, Mills and Ma [3] modelled angle legs of a steel lattice tower and studied increasing the load resisting capacity by providing reinforcement. At present, there are two main reinforcing methods that are used in practice for lattice transmission

towers. The first method involves providing a number of horizontal braces along the height of tower mainly on members that are under compression load. The second method involves improving the capacity of the existing members by retrofitting them with reinforcement members. Authors investigated the most effective leg retrofitting method with experimental and nonlinear FEM phases. Three specimens were tested and their results were compared with FEM results. Among the connection types examined for the intermediate joints, the cruciform type provided the highest average strength increase with large standard deviation and FEM model result was coincided with that.

Puthli and Fleischer [4] tested twenty-five bolted connection specimens with different bolt spacing and edge distance. Bolted connections were of single shear type as the case in this thesis and all calculations were designed using Eurocode-3. Deformations were observed on regions around the bolt before the occurrence of rupture. The results of this work showed that a reduction of the design bearing capacity is not required for edge distance $e_2 \geq 1.2\ d_o$ or bolt spacing $p_2 \geq 2.4\ d_o$. In addition to this, minimum edge distance may be reduced to $0.9d_o$ and minimum bolt distances may be reduced to $1.8d_o$.

Xie and Sun [5] tested three pairs of steel lattice tower subassemblies with diaphragms to investigate failure mechanisms of the structure under simulated wind and ice loads. Authors selected a 500-kV transmission tower with a height of 48.5 m for their prototype design. Because of the space limitation of laboratory, structure was scaled. Design of structure was done according to Chinese Code (NCETC 2002). The results of this work show that buckling of main legs was the primary failure mode of structures under lateral and vertical loads. Using diaphragms was shown to provide benefits on structure by increasing the load carrying capacity.

Salih, Gardner and Nethercot [6] performed numerical and experimental studies for stainless steel connections using EN 1993-1-4 and EN 1993-1-8. Net section rupture of single angles connected by one leg to a gusset plate with a single row of bolt was researched. FEM models were also created and their results were compared with experimental results. It was seen that both results validated each other. There were

three important parameters for net section capacity and these were number of bolts, spacing between bolts in the direction of loading and eccentricity of the connection. Connection eccentricity was reported to have a significant influence on the ultimate strength of the net section with the capacity being decreased with increasing eccentricity. Numerical and experimental results suggested that net section resistance is often under-predicted by design codes.

Lu, Ma and Mills [7] studied structural effects of bolted splices on retrofitted transmission tower angle members. Aim of the study was to investigate the structural behavior of built-up members which are used for steel leg of transmission towers. The legs have been retrofitted by additional parallel angle members. This study includes both experimental four specimens and two numerical model tests results. Load capacity was increased using additional parallel angle members. For this study, compression load was applied on specimens and numerical models. Importance of the interior and exterior reinforcement angle member under compression load was investigated. It was showed that the bolt-splice joint and bolt connector played a critical role in the structural behavior of the bolt spliced reinforced member. In addition, ultimate load carrying capacity was increased by reduction in slip-load of the middle splice-joint and an increase in slip-load of top connector. Load transfer between original members and additional reinforcing components was observed and experimental and numerical studies validated each other.

Chesson and Munse [8] worked on behavior of large riveted and bolted structural connections. Net section area, geometrical efficiency factor, bearing factor, shear lag factor and ductility factor was reported to influence the test efficiency of connections failing on net section. Orientation of the specimens and testing machine affected deformation characteristics, and distance between specimen and testing machine caused eccentricity, so ultimate strength of material decreases. The shear lag effect was evident in the connected legs and outstanding legs of angle members. Deformations in punched members were generally smaller than drilled members and deformation of bolted members were generally smaller than riveted members, so using punched members could be useful. In addition to these, short joints provide a less favourable stress transfer. As a result, gusset plates are not always fully effective

according to their entire width and this should be considered for design procedure. Punched members are only 85-90% as effective as similar drilled members. According to Chesson and Munse "An upper limit should be placed on the maximum portion of the gross area which may be considered effective in resisting a tensile load." A reduction constant of 0.9 was recommended.

1.3. OBJECTIVE AND SCOPE OF THE STUDY

The main objective of this study was to experimentally investigate the behavior of bolted splice connections of lattice overhead transmission line towers under tension loading. Seven specimens with each of them having a different connection detail were tested. The main parameters used in the testing program were the number of bolts used in the connection, presence of connection reinforcement angles, and the number and geometry of filler plates used between the main members. The study aimed at: (1) better understanding the load-flow mechanism in the connection, (2) determining the "redundant" members in the connection, and (3) simplifying the connection geometry by eliminating the redundant members

1.4. ORGANIZATION OF THESIS

This thesis is divided into three chapters. Following this introduction part is Chapter 2, which presents experimental study and results. Chapter 3 is summary of this thesis. This chapter includes conclusions and recommendations for further study. Specimen design calculations can be seen in Appendix A.

CHAPTER 2

EXPERIMENTAL STUDY

2.1. GENERAL

In total, seven tension splice connection specimens were tested as part of this study. All specimens were fabricated in production facility of Mitas Energy and Metal Construction Inc., and were tested at Atilim University Structural Mechanics Laboratory. The specimens were fabricated using S355 grade steel material and a different connection detail was tested with each specimen. Overall goals of the experimental study were (1) to better understand the connection behavior by identifying the load-flow mechanism, and (2) to identify the redundant members in the connection and simplify the connection geometry by eliminating these redundant members.

2.2. TEST SPECIMENS

A prototype latticed transmission tower was designed and the splice connection at main legs of this prototype structure was used as a basis for the test specimens. The prototype tower has a height of 75 m and a capacity of 500 kV. Loads used for the design included wind and ice loads, installation and repair loads, equipment and conductor loads, earthquake load, and broken wire load. A commercial computer program (PLS-Tower) was used to create the tower geometry, to apply the loads on the tower, to analyze the tower under loads, and to specify the member sizes. A view of the prototype tower is given in Figure 2.1. The main leg splice connection indicated on the figure was investigated in this study. Design of the tower is based on S355 grade steel angles and 8.8 grade bearing type bolts.

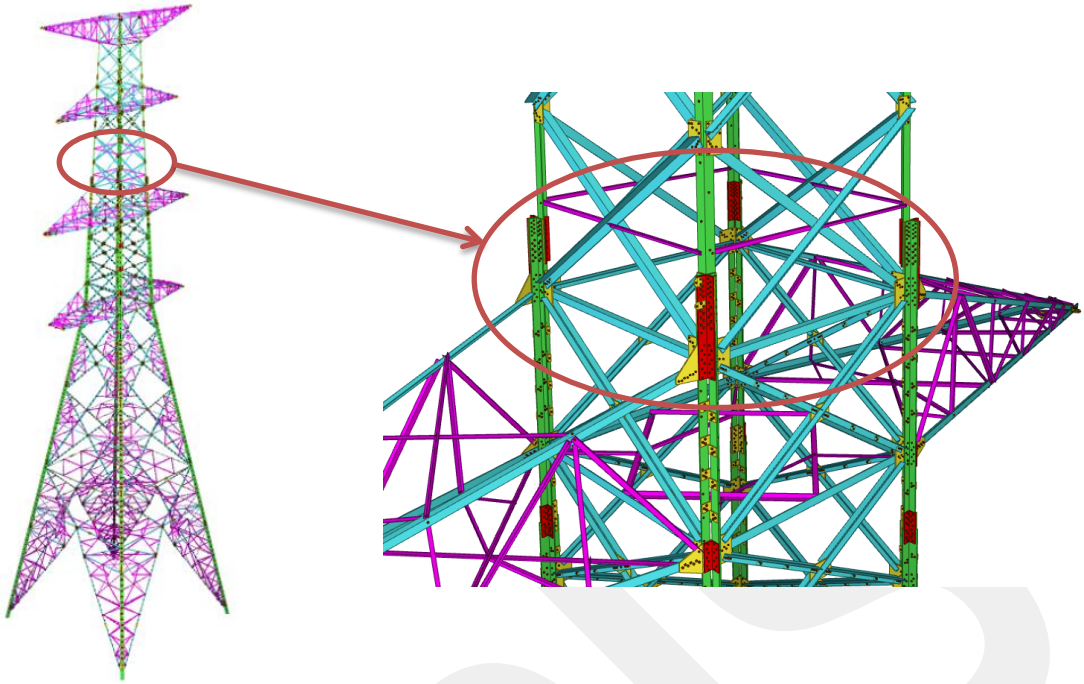

Figure 2.1. 3D tower model and connection part of structure

Investigated connection part of tower is called “cruciform type connection”. For this type of connection, the number of angle sections used in each main leg member can change from one to four according to carried load. For the prototype tower, two main angle arms (corner to corner) come from bottom of tower, then one angle arm continues to top. Based on this connection layout, the geometries shown in Figure 2.2 were investigated in this study. Layout of the geometry used in each specimen is also explained in Table 2.1. Each specimen contained an upper main member, two lower main members, additional reinforcement angle members and filler plates used for the connection. Additional reinforcing plates were welded to the free ends of upper and lower main members to compensate for the loss of capacity due to bolt holes existing at these locations. As shown, the main variable among the test specimens was the presence of interior and exterior reinforcement angle members and filler plates. Geometric details of the connection elements used in the test specimens are given in Figures 2.3-2.8. The main members in the prototype tower were made of L150x16 angle section for lower main members and L160x17 angle section for upper main member. However, due to the limited capacity of testing machine actual scale members could not be used. Because of this reason, specimens were prepared with 1/7.5 scale and L60x6 angle section was used for the main

members. L60x6 section has the same width/thickness ratio as the L150x16 and L160x17 sections of the prototype tower. Detailed design calculations for the test specimens are provided in Appendix A part of thesis.

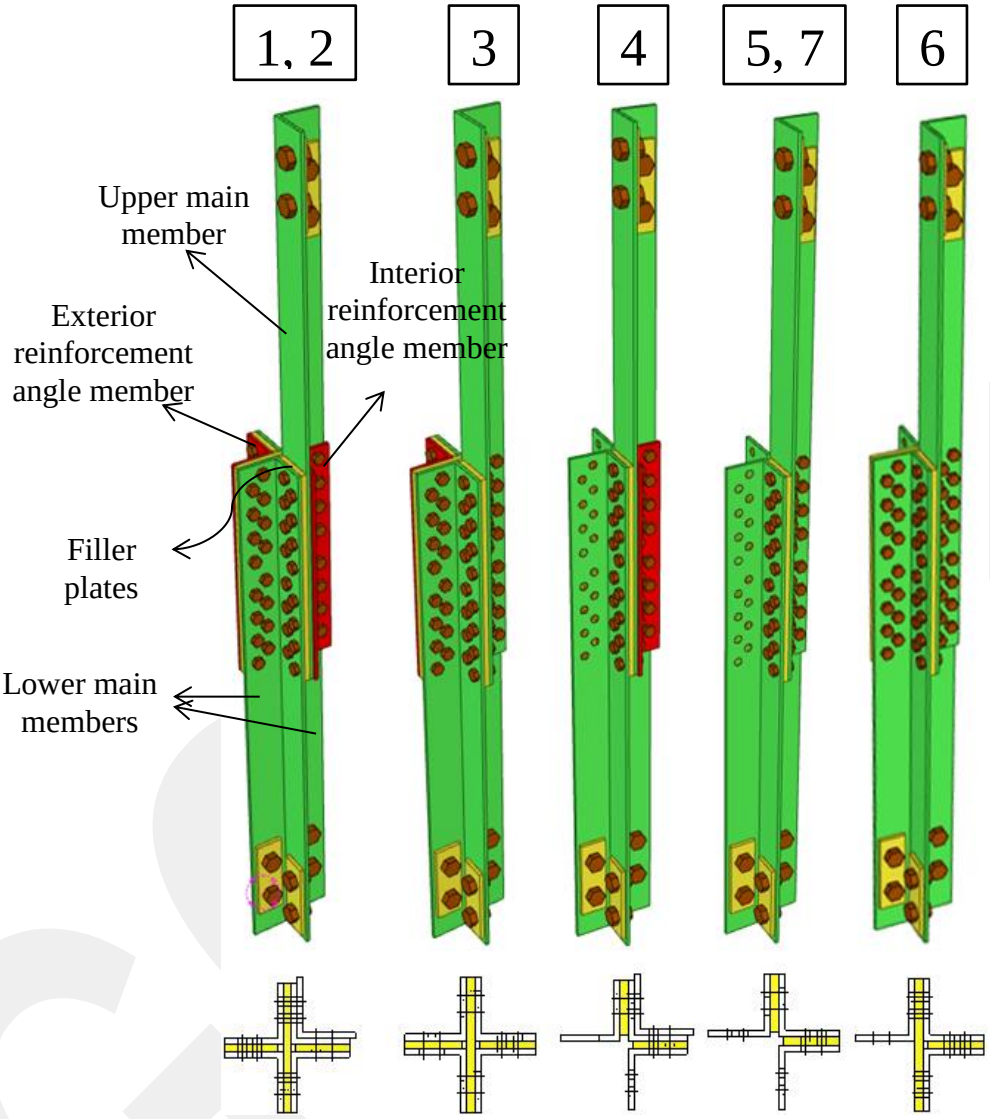

Figure 2.2. Overall geometry of test specimens

Table 2.1. Details of connection layouts used in test specimens

Specimen Number	#1	#2	#3	#4	#5	#6	#7
Interior Reinf. Mem.	Yes	Yes	No	Yes	No	No	No
Exterior Reinf. Mem.	Yes	Yes	Yes	No	No	No	No
Long Filler Plate	Yes	Yes	Yes	No	No	Yes	No
Short Filler Plate	Yes	Yes	Yes	Yes	Yes	Yes	No*
Bolt Size	M7	M8	M8	M8	M8	M8	M8

* Small pieces of plate washer were used instead of a filler plate.

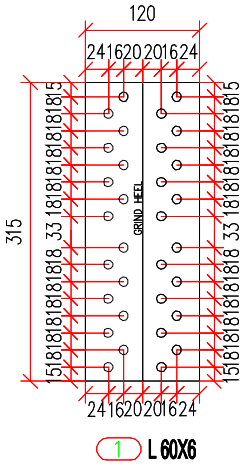

Figure 2.3. Interior reinforcement angle member (dimensions in mm unit)

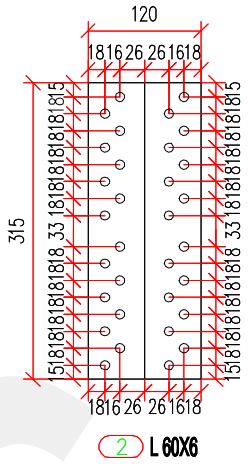

Figure 2.4. Exterior reinforcement angle member

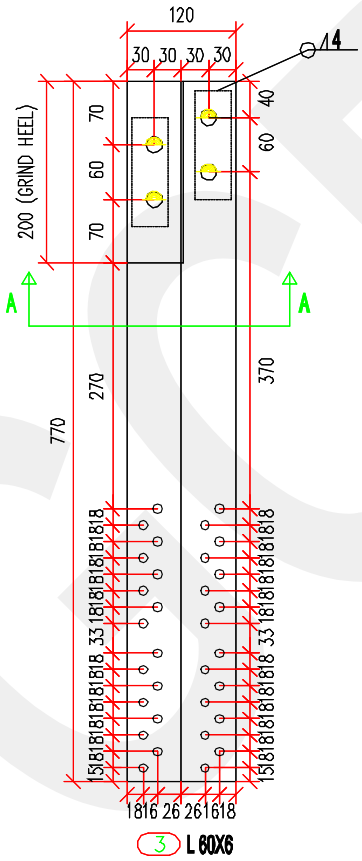

Figure 2.5. Upper main member

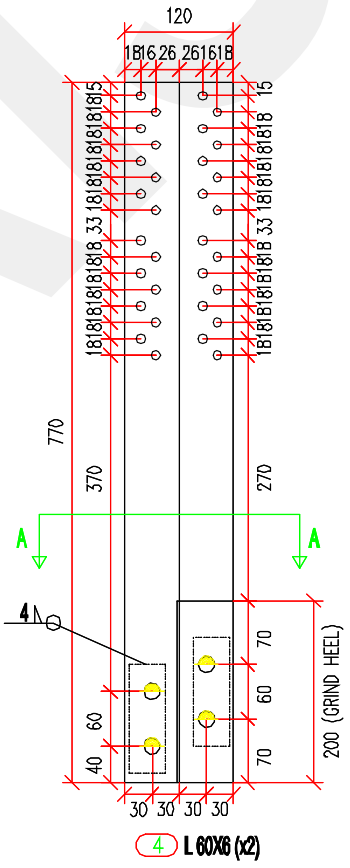

Figure 2.6. Lower main member

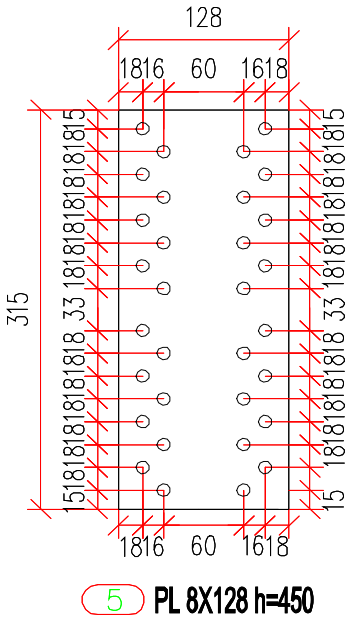

Figure 2.7. Long filler plate

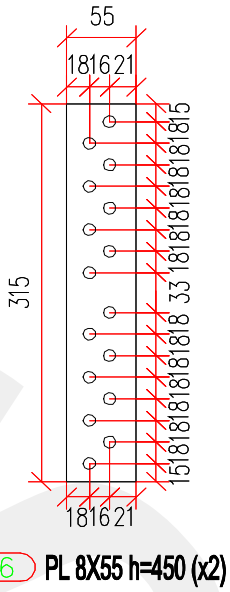

Figure 2.8. Short filler plate

Tension tests were performed on coupon samples that were cut from upper main member in Specimens 1, 2, 4, 5, and 6. Pictures of coupon samples and testing procedure are shown in Figure 2.9. By this way, yield and ultimate strength values were determined, and are given in Table 2.2.

Figure 2.9. Tension test coupons and testing procedure

Table 2.2. Coupon tension test results

	F_y (MPa)	F_u (MPa)
Specimen 1	400	525
Specimen 2	398	506
Specimen 4	391	500
Specimen 5	380	483
Specimen 6	356	470

2.2.1. Test Setup and Testing Procedure

As shown in Figure 2.11 testing device included a hydraulic actuator that had a load cell and two swivel heads attached. The lower end of the specimen was attached on the testing frame and vertical upward displacement was applied at the upper end with the actuator. Displacement loading was applied with a constant rate of 0.02 mm/s until the failure of specimen, which was either fracture of the upper main member or fracture of the bolts. Strain gages were used in some specimens and they were placed on the predetermined locations. In addition to this, a displacement transducer was used to measure the relative displacement between points A and B indicated in Figure 2.12. These points were spaced equally from the connection region and the distance between them was equal to 50 cm. The load cell, strain gages, and displacement transducer were connected to a data acquisition system (see Figure 2.10) and the readings were continuously collected and recorded during load tests.

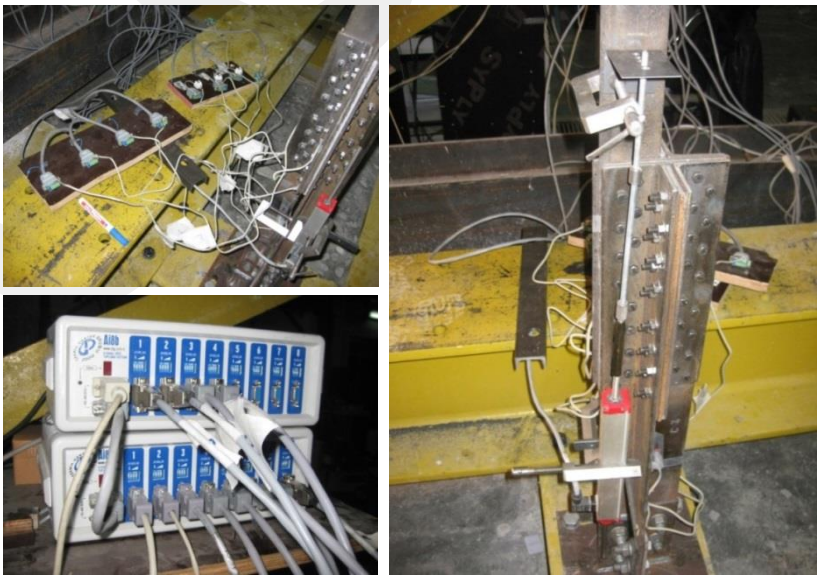

Figure 2.10. Strain gages, displacement transducer, and data acquisition system

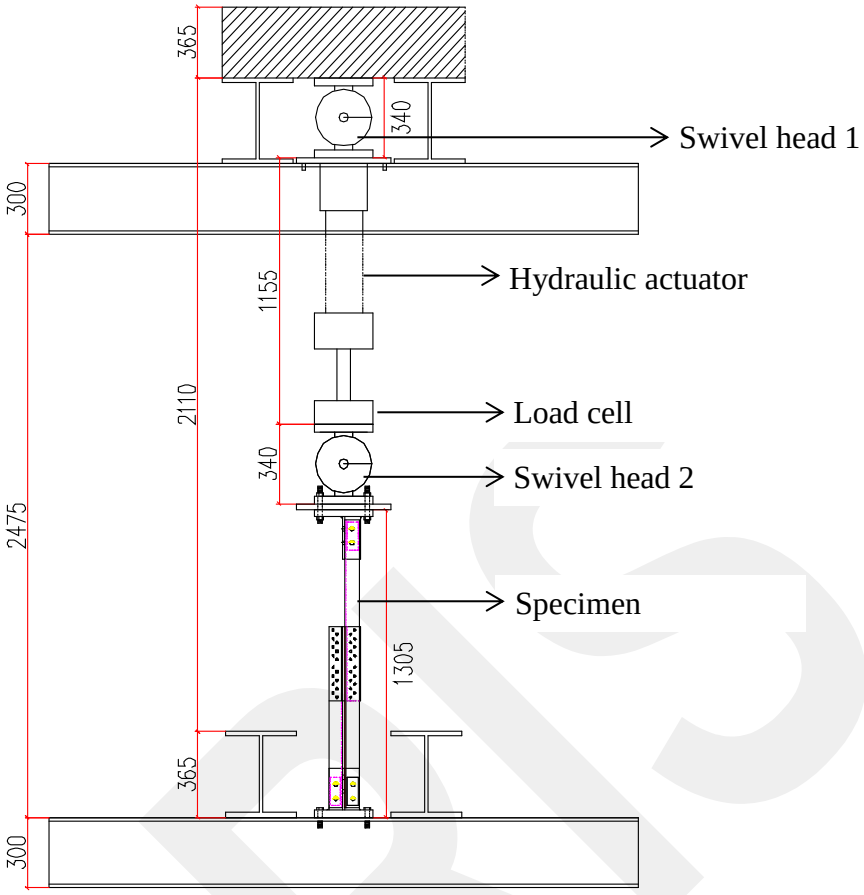

Figure 2.11. Testing device and parts of the system (dimensions in mm unit)

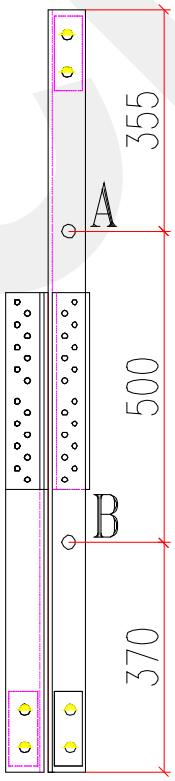

Figure 2.12. Displacement transducer location (dimensions in mm unit)

2.2.2. Specimen-1

General views and geometric details of the connection region in Specimen-1 are given in Figures 2.13 and 2.14, respectively. Different from the other specimens, 7 mm diameter (M7) bolts are used in this specimen. This detail represents the connection that is currently being used in the industry for splice of main member angle sections in steel latticed transmission towers. Both interior and exterior reinforcement angles were used in the connection. The connection also included two pieces of short and one piece of long filler plates, and sixty-four bolts in total.

Figure 2.13. Members and connection detail of Specimen-1

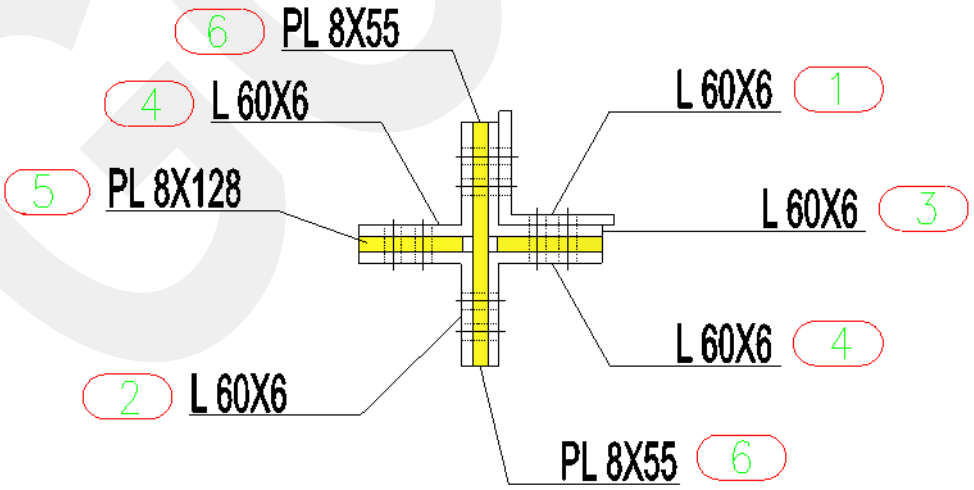

Figure 2.14. Cross-sectional view of Specimen-1

Rupture of all of the sixteen bolts between one leg of the upper main member and one of the lower main member occurred at a load of 263.7 kN (Figure 2.15). As indicated in Figures 2.16-2.17, shear type deformation was observed on the bolts attached on the other leg of the upper main member. Capacity calculations performed prior to the load test indicated the fracture at net cross section in the upper main member to be the governing failure mode with an estimated capacity of 274.1 kN. These calculations were based on the assumptions of (1) pure shear condition in the bolts and (2) bolt threads being excluded in the shear plane. It should be noted here that the M7 bolts used in this specimen had fully-threaded shank part, which means that the effective diameter resisting the bolt force was actually smaller than 7 mm. Moreover, bending type of deformation was observed in the upper and lower main members (see Figure 2.18), and such deformation is an indication of the presence of tension load in the bolts, in addition to the shear. These two factors are believed to be the reason for having bolt failure in this specimen, even though the expected failure was net section fracture of the upper main member. Examination of the upper main member after the load test indicated that necking has started at the critical path and bearing deformation occurred on the bolt holes located along this path (Figure 2.19).

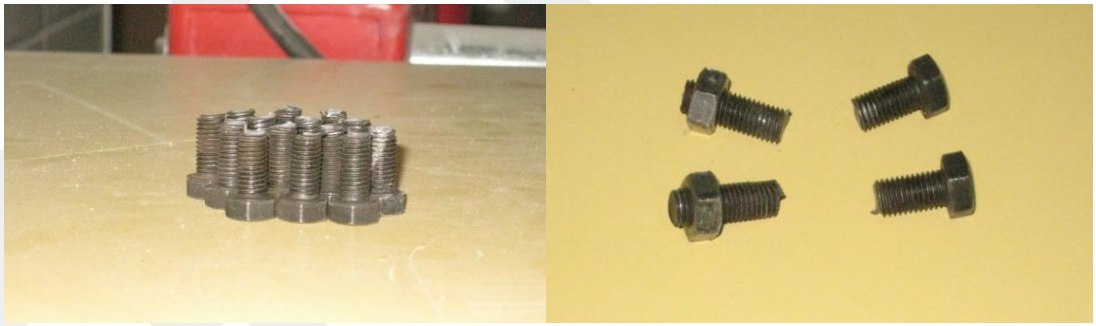

Figure 2.15. Ruptured bolts of Specimen-1

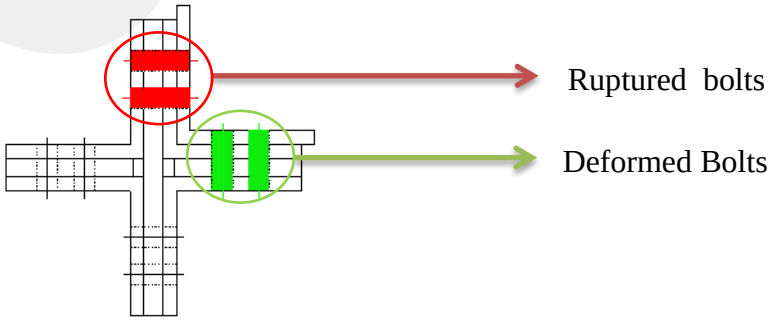

Figure 2.16. Location of deformed and ruptured bolts

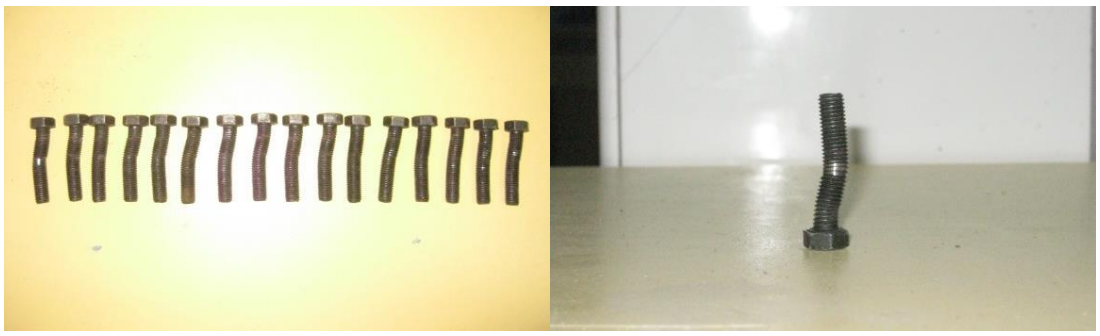

Figure 2.17. Deformed bolts of Specimen-1

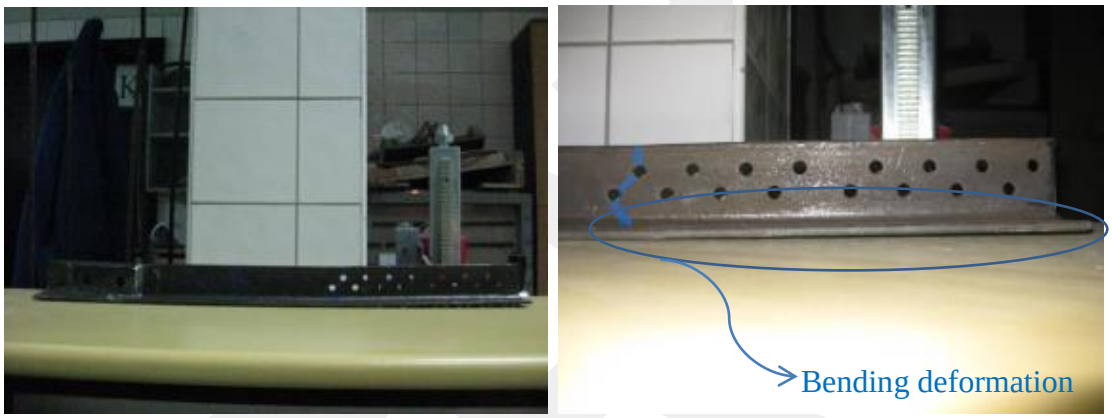

Figure 2.18. Bending on upper main member of Specimen-1

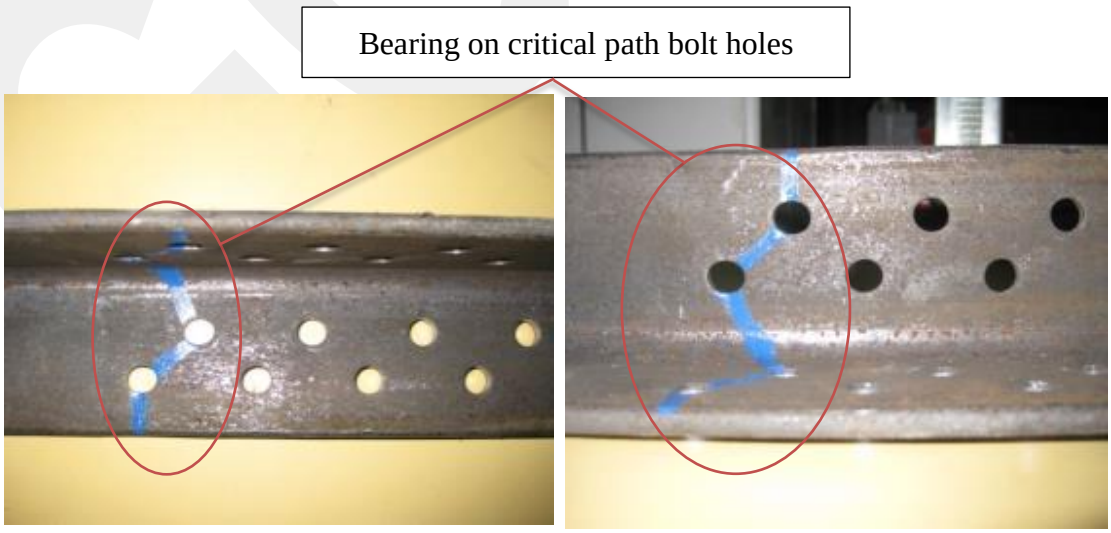

Figure 2.19. Critical path and bearing on bolt holes (Specimen-1)

Additional direct tension and micro-hardness tests were conducted on samples of M7 bolts in order to verify that the material grade was actually 8.8. After the testing, it was seen that all bolts have 8.8 grade property as indicated by the test report shown in Figure 2.20.

Yield Stress is expected min 640 MPa,
Ultimate Stress is expected min 800 MPa for 8.8 grade bolts.

S/N	σ_y (MPa)	σ_u (MPa)
Specimen 1	801	887
Specimen 2	799	859
Specimen 3	813	879

Micro hardness is expected min 22 HRC and max 32 HRC for 8.8 grade bolts.

S/N	Measurement 1 HRC	Measurement 2 HRC	Measurement 3 HRC	Average HRC
Specimen 1	28.3	27.8	28.5	28.2
Specimen 2	30.5	29.7	28.7	29.6

According to these test results, all bolts have 8.8 grade property.

Figure 2.20. Test results of M7 bolts

Measured load-displacement response of Specimen-1 is given in Figure 2.21. Load values shown on the plot indicate the load applied by the actuator at the top end of the upper main member, while the displacement values represent the relative displacement between points A and B shown in Figure 2.12. Calculated capacities corresponding to yielding on gross cross section, yielding on net cross section, and fracture on net cross section of the upper main member are also shown on the same plot. It should be noted that these calculated values are based on the assumption of pure axial force in the main members. Therefore, presence of bending in these members would violate this assumption and result in capacities different than these predicted ones.

As mentioned previously, load testing of this specimen was terminated when some of the bolts in the connection region were fractured. For this reason, a direct comparison between the measured load capacity and the predicted load capacity corresponding to fracture on net cross section of the upper main member is not possible. On the other hand, measured and predicted load capacities in terms of yielding can be compared. The load at which the initial slope of the load-displacement curve started to change

can be taken as the load causing initiation of yielding. Value of this load is approximately 88.3 kN for Specimen-1, and it is significantly lower than the predicted load level corresponding to yielding on net cross section.

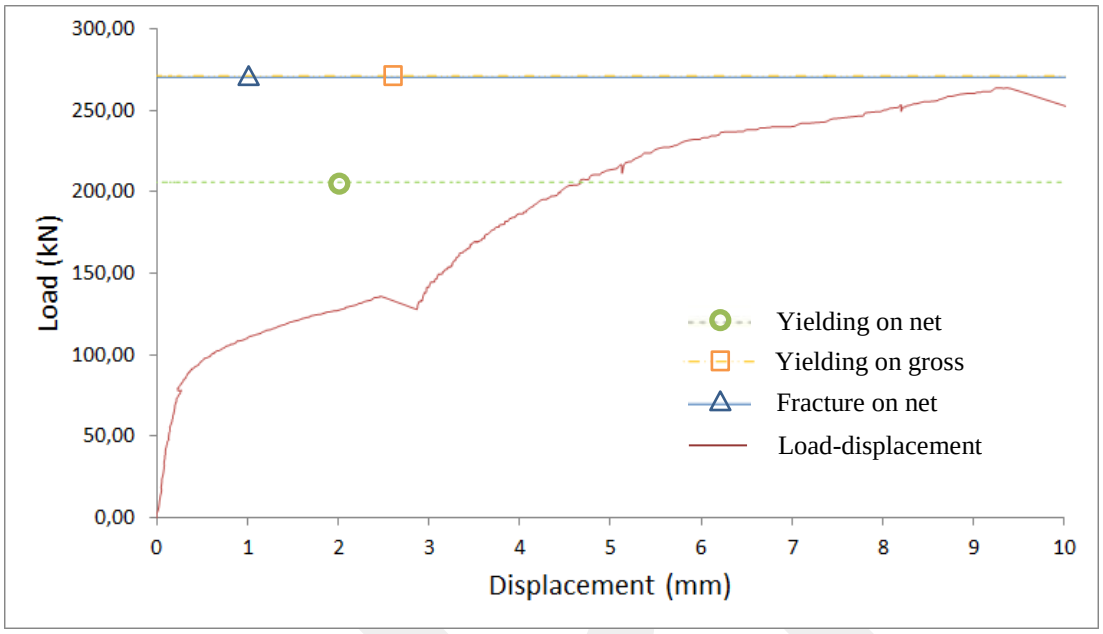

Figure 2.21. Load-displacement behavior for Specimen-1

Strain Gage Readings

The main members and interior reinforcement angle in Specimen-1 was instrumented with totally ten strain gages, as shown in Figure 2.22. Readings from these gages were used to determine the strain distribution at different parts of the specimen.

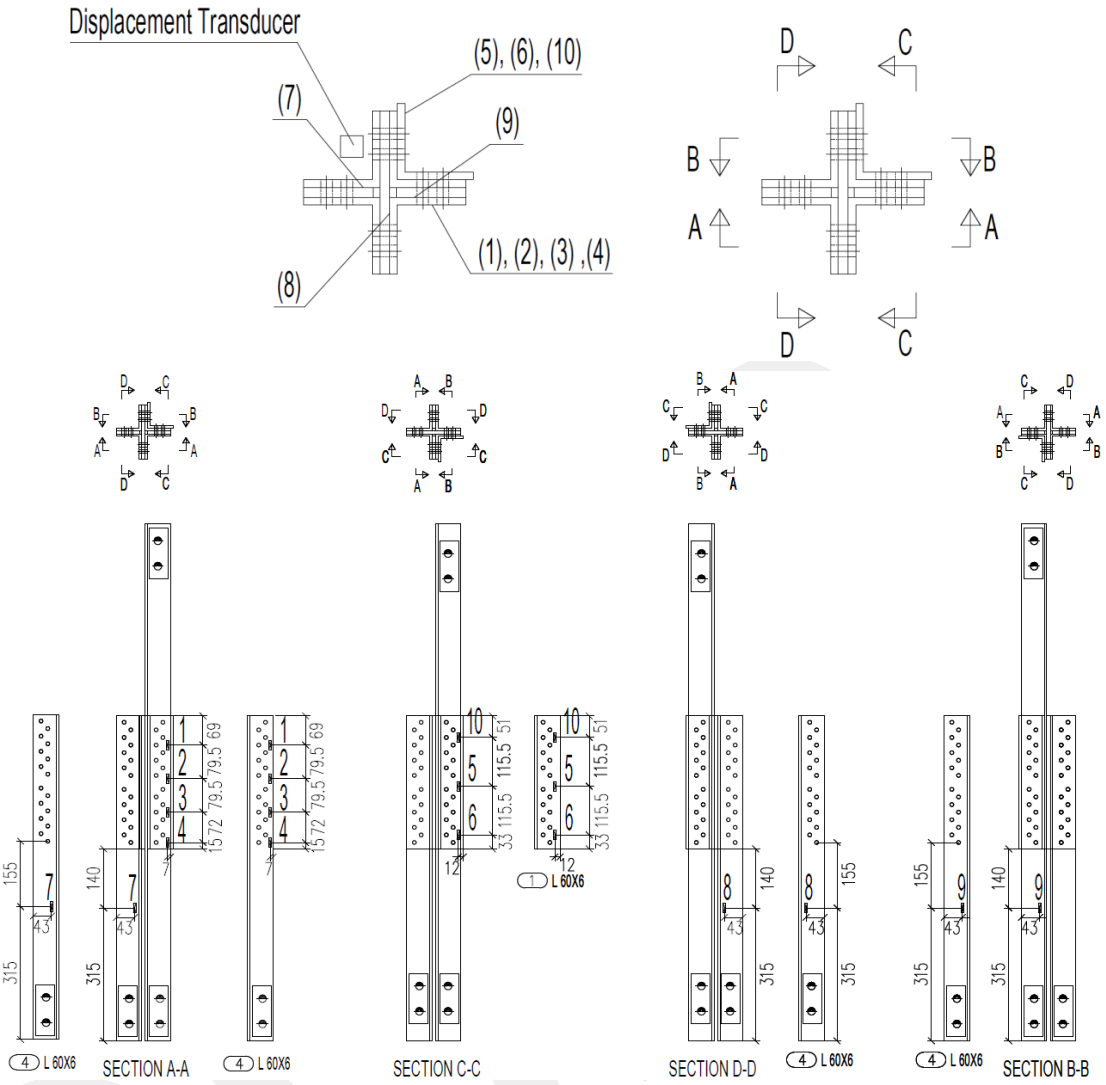

Figure 2.22. Strain gage and displacement transducer locations in side and cross-sectional view of Specimen-1 (dimensions in mm unit)

- **Strain Distribution in Lower Main Members**

Variation of strain indicated by Gages 1, 2, 3, and 4, which were placed on one of the lower main member, is shown in Figure 2.23. Gage 4 was located at the most critical cross section of this member and Gage 1 was farthest away from the critical cross section. The plots clearly show the trend that the tensile strain decreases as the distance from the critical cross section increases. This is an expected result, because starting from the critical cross section the load in the lower main members is transferred to the upper main member by the bolts. Starting from a load of approximately 220.7 kN, the rate of strain change in Gage 4 increases. This is an indication of yielding at the critical cross section at this load level. It should be noted

that this is the total load applied by the actuator. Assuming that the two lower main member angles share the load equally, the load in each angle section becomes 110.4 kN. This level of load is significantly smaller than the predicted load of 208.8 kN corresponding to yielding on net cross section. This observation also indicates the presence of bending deformation in addition to the axial deformation of the lower main members.

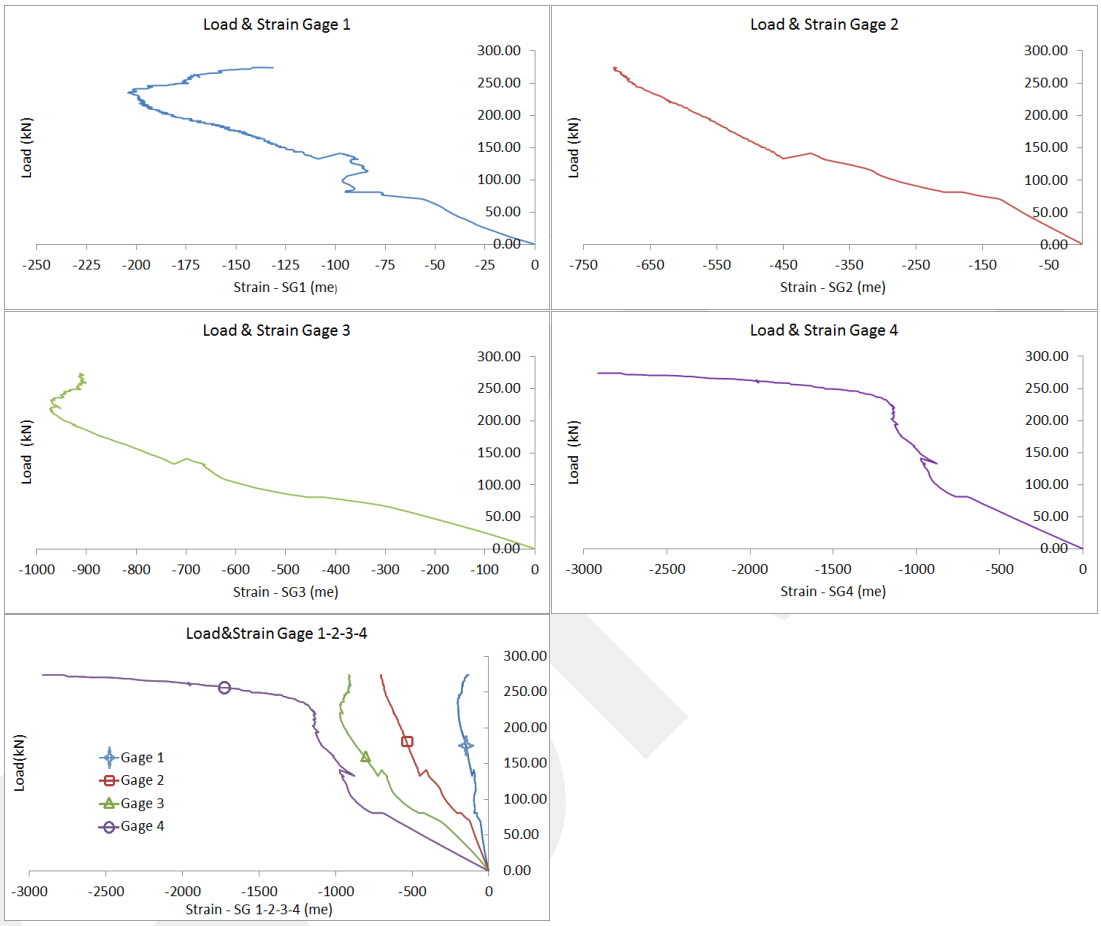

Figure 2.23. Strain distribution in lower main member of Specimen-1

Readings from Gages 1-4 were also used to extract the strain profile on one of the lower main member at different load levels. These profiles are given in Figure 2.24. The plots indicate that the strain profile remained almost linear up to a load level of 220 kN, and after this level the rate of change of strain at the most critical section (indicated by Gage 4) started to increase. It should again be noted that the load values shown on these plots are the total load applied by the actuator. Load in each lower main member would be expected to be half of the total actuator load.

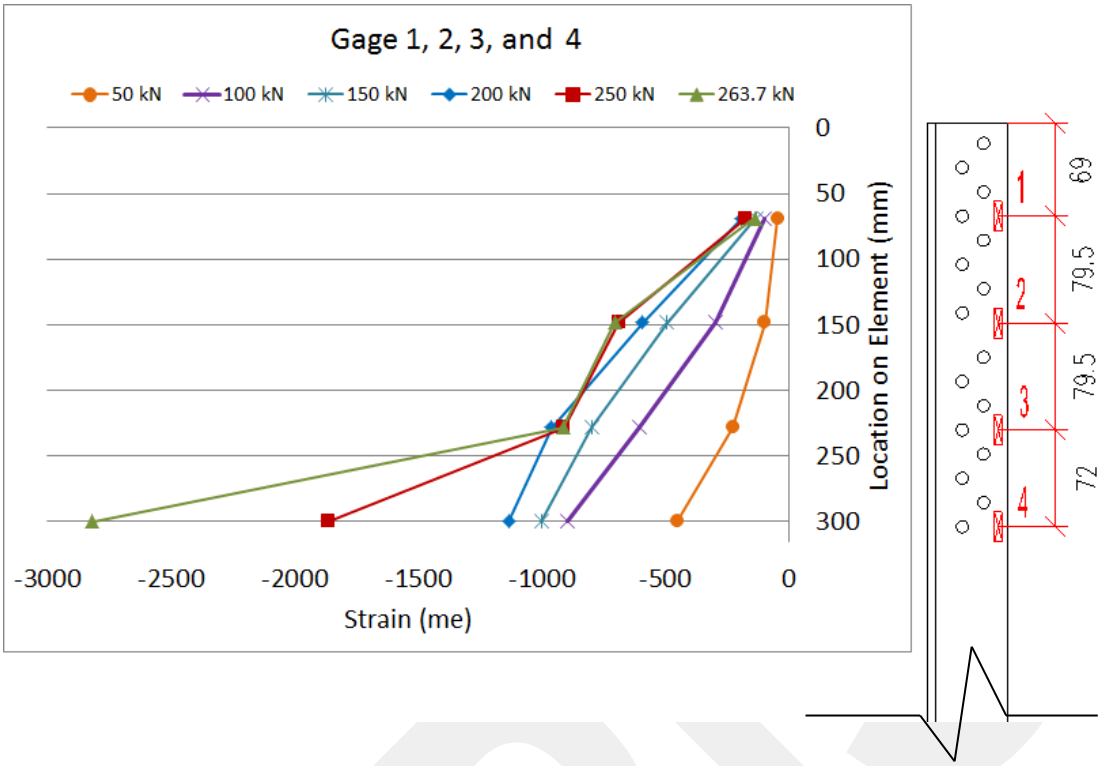

Figure 2.24. Variation of strain profile in lower main member of Specimen-1 (dimensions in mm unit)

Gages 8 and 9 were located on two legs of one of the lower main member, while Gage 7 was located on one leg of the other lower main member. These three gages were located at cross section away from the connection region. Location of all of these three gages on the leg of the angle section as well as the distance from the end of the member was the same. Readings from these gages are shown in Figure 2.25. The fact that the strain readings from these three gages are different from each other is another indication that the lower main members are not under pure axial tension loading. Another reason that the strain readings from Gages 8 and 9 are different from each other is related with the shear lag effect in the lower main members. Only one leg of each lower main member is connected to the upper main member. Therefore, near the connection region, the strain in the leg that was connected to the upper main member would be expected to be larger than the strain in the other leg, which had no direct connection. This is justified by the condition that Gage 9 indicated larger strains than Gage 8.

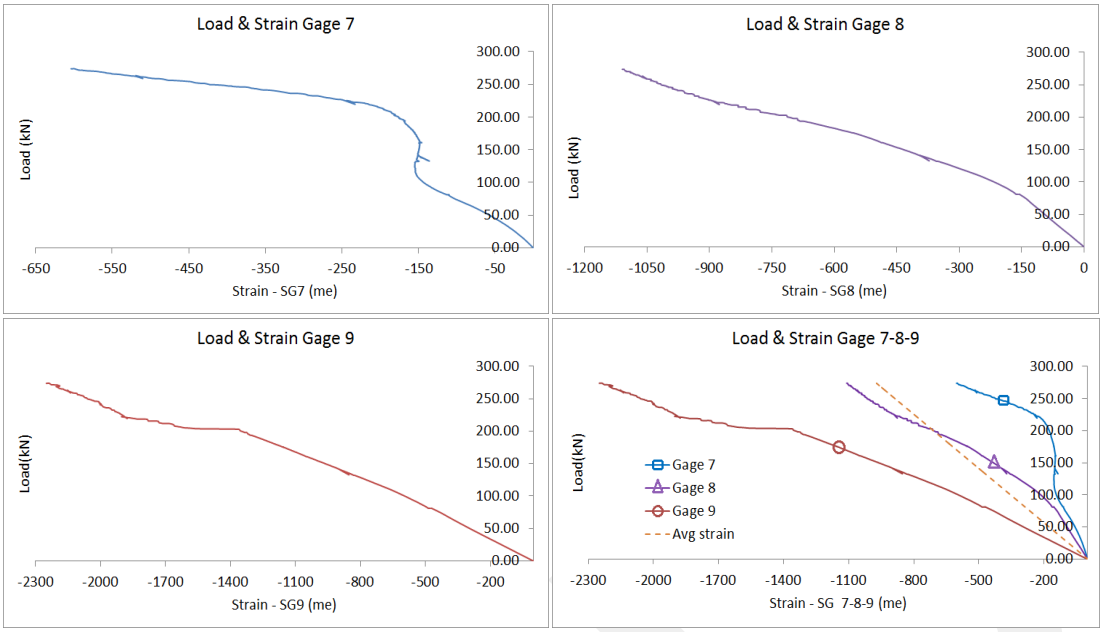

Figure 2.25. Comparison of strains in lower main members of Specimen-1

- **Strain Distribution in Interior Reinforcement Angle**

The interior reinforcement angle was instrumented with three strain gages (Gages 5, 6, and 10). Readings from these gages are shown in Figure 2.26. Assuming that the member itself will be subjected to tensile load, the strain gages would be expected to indicate only tensile strain. The plots, on the other hand, indicate that Gages 6 and 10, which were located at two ends of the interior reinforcement angle recorded both tensile and compressive strains. The reason for this is believed to be bending of the interior reinforcement angle together with the upper and lower main members. Such bending deformation was evident in the upper and lower main members following the load test. The main reason for this additional bending deformation was the eccentricity of the load acting on the angle members with respect to the centroidal axis of each member.

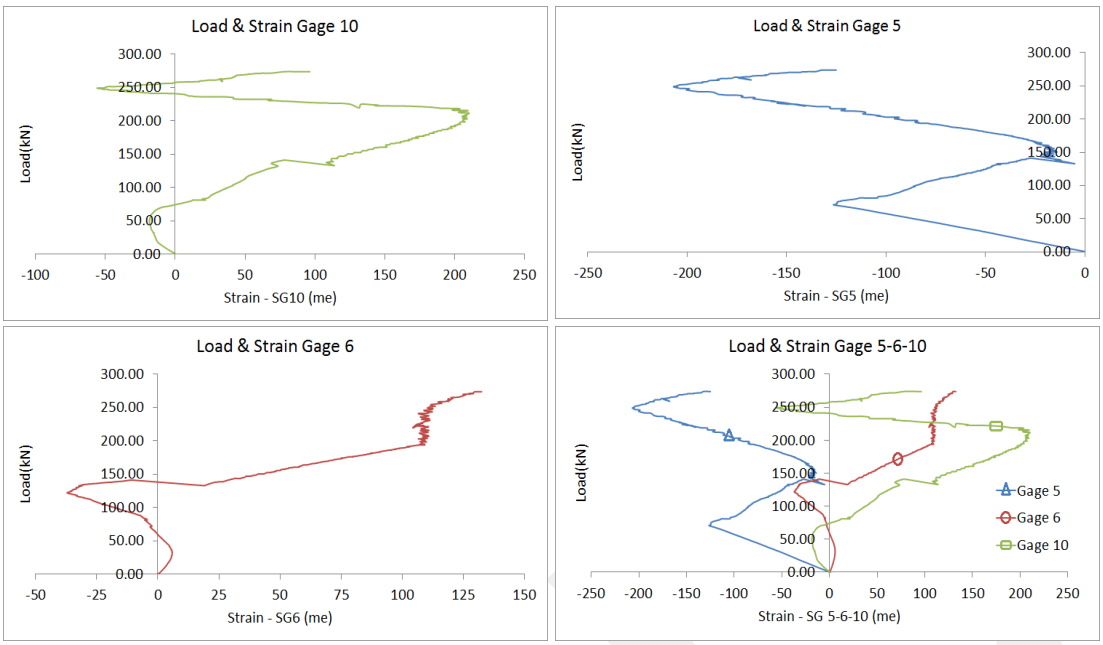

Figure 2.26. Strain distribution in interior reinforcement angle of Specimen-1

The unexpected distribution of strains in the interior reinforcement angle as a result of additional bending deformations can also be seen clearly on the strain profiles shown in Figure 2.27.

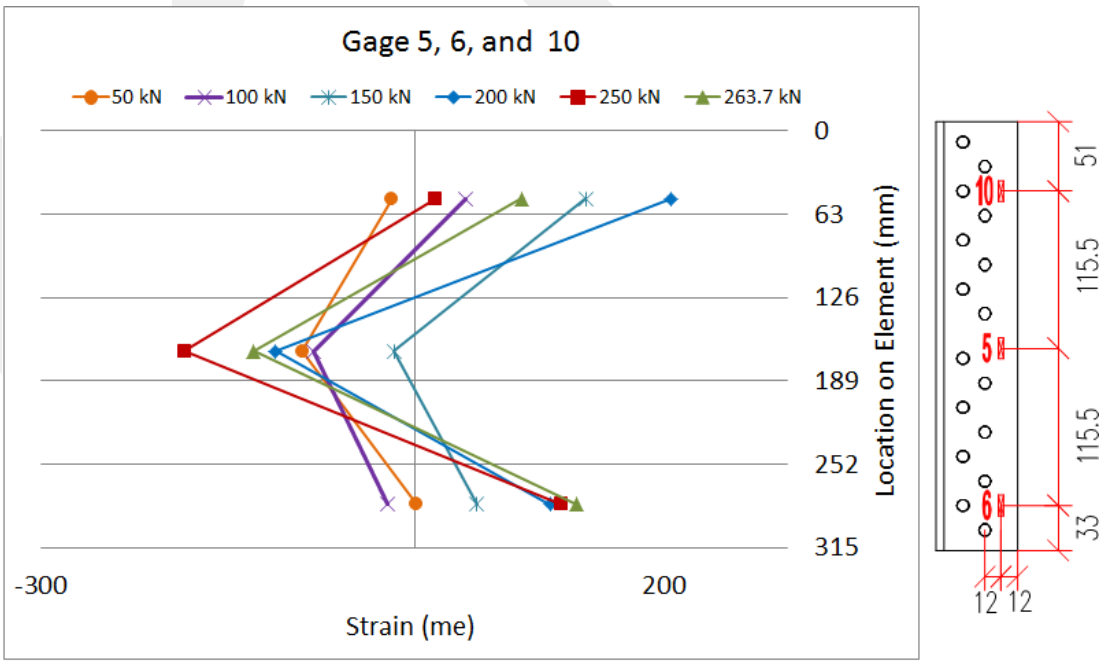

Figure 2.27. Variation of strain profile in interior reinforcement angle of Specimen-1 (dimensions in mm unit)

2.2.3. Specimen-2

In order to prevent the bolt failure occurred on Specimen-1, M7 bolts were replaced by M8 bolts with threads excluded from the shear plane. Other than this difference in the bolts, the connection details used in Specimen-2 was the same as those in Specimen-1. The connection included sixty-four bolts in total. General views and geometric details of the connection region in Specimen-2 are given in Figures 2.28 and 2.29.

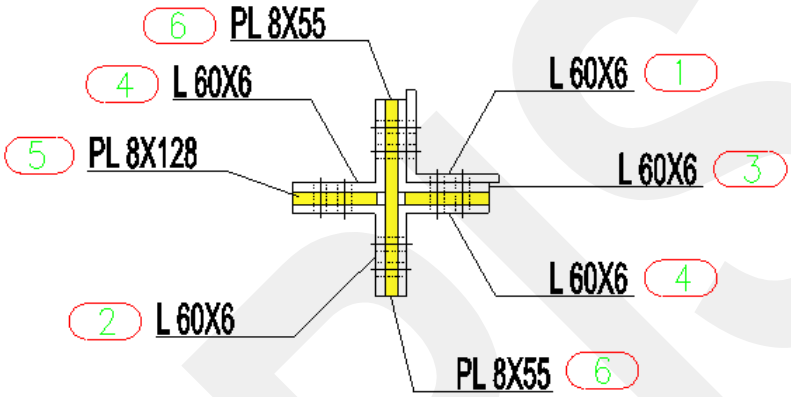

Figure 2.28. Cross-sectional view of Specimen-2

Figure 2.29. General views of Specimen-2

According to the hand calculations, upper main member was expected to rupture on critical path in 264.1 kN of loading. During load testing the member underwent net section fracture along the first line of bolts at a load of 254.4 kN (see Figure 2.30). Analysis of the upper main member after the load test indicated bearing on bolt

holes, necking on the artificial cross section, and overall bending deformation of the member, as seen on the pictures given in Figure 2.31.

Figure 2.30. Rupture on critical path of Specimen-2

Figure 2.31. Deformations on ruptured angle member of Specimen-2

Reinforcement angle members and filler plates were analysed and as shown in Figure 2.32, and no deformation was observed on these elements.

Figure 2.32. Reinforcement angle members and filler plates of Specimen-2, after testing

Two lower main members were analysed and bending was detected. A schematic illustration of the deformed shape of the specimen is shown in Figure 2.33. Pictures showing the deformation of the lower main members are provided in Figures 2.34 and 2.35. As mentioned previously, this type of bending deformation occurred because of the eccentricity between the line of application of the load and the centroid of the angle members.

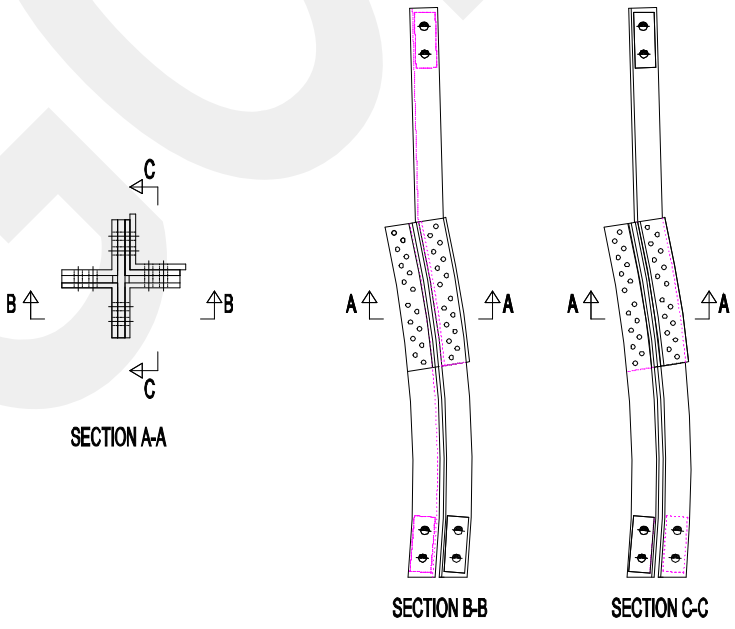

Figure 2.33. Exaggerated deformed shape of specimen

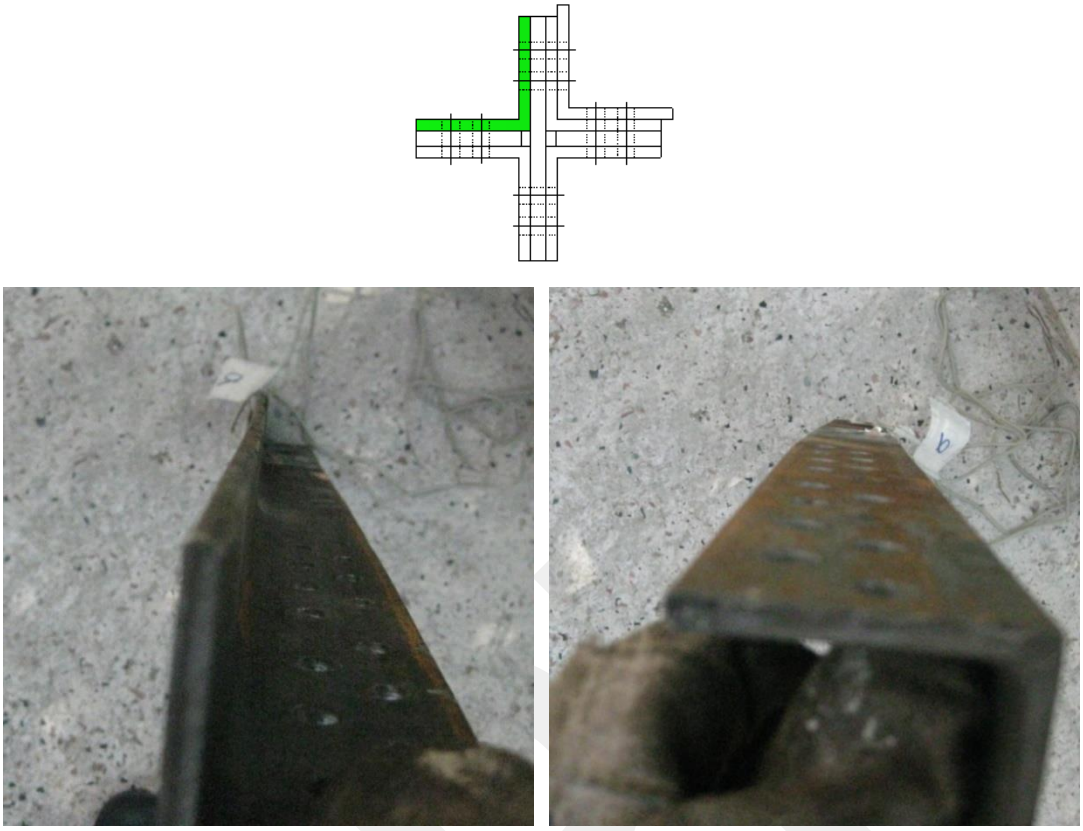

Figure 2.34. Bending on lower main member 1 (Specimen-2)

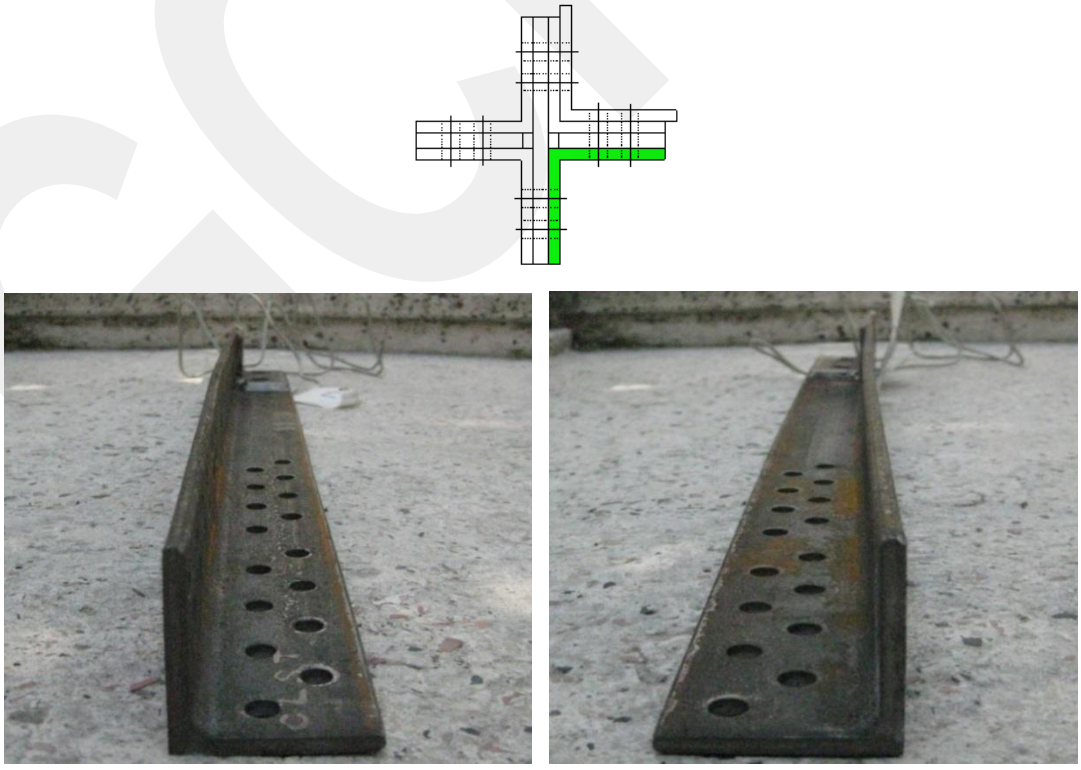

Figure 2.35. Bending on lower main member 2 (Specimen-2)

As shown in Figures 2.36 and 2.37, bearing on critical path bolt holes was also observed on lower main members. Inspection of the bolts following the load testing of Specimen-2 did not indicate any type of bolt deformation.

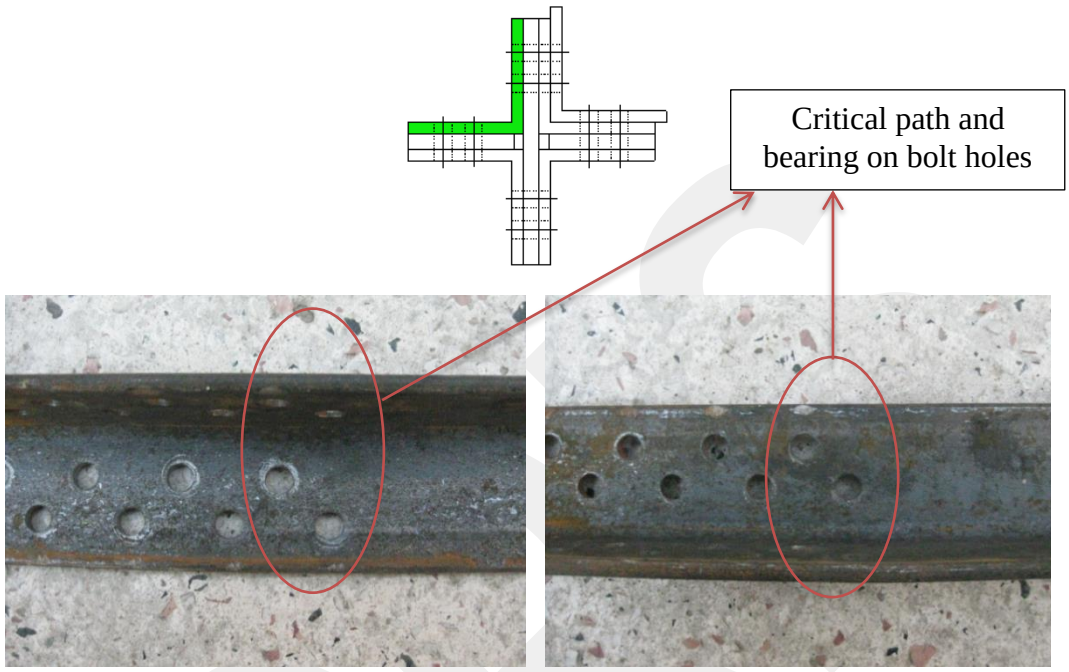

Figure 2.36. Bearing on lower main member 1 (Specimen-2)

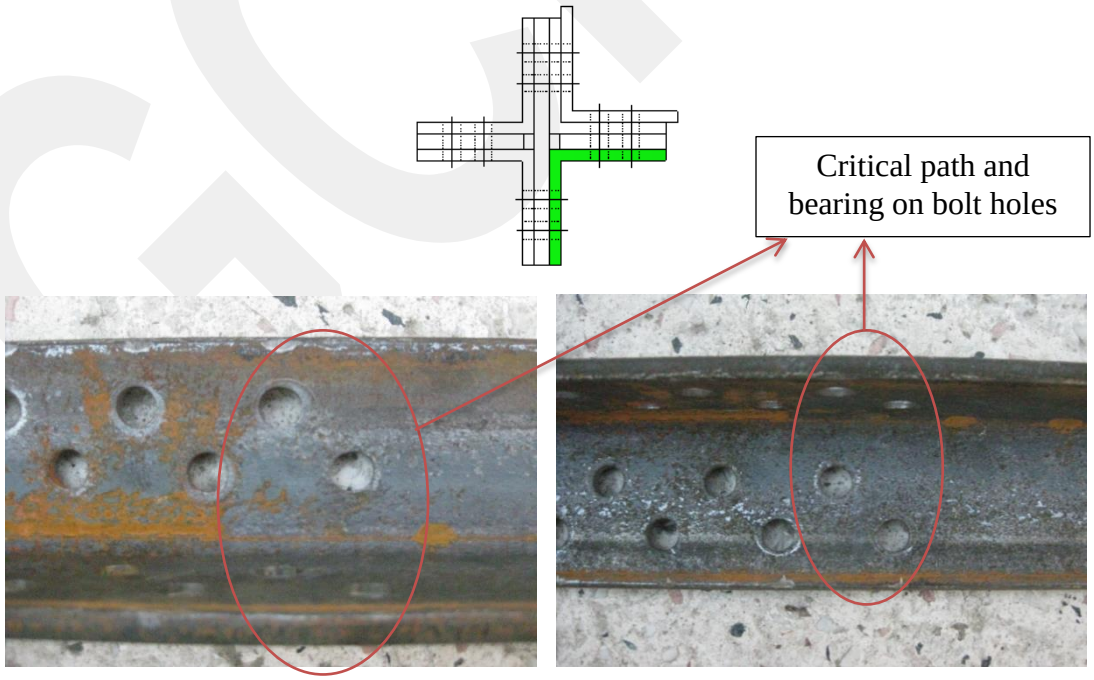

Figure 2.37. Bearing on lower main member 2 (Specimen-2)

Measured load-deformation behavior of Specimen-2 is shown in Figure 2.38. The relation between the predicted load capacities corresponding to yielding on net section, yielding on gross section and fracture on net section, and the measured response of the specimen can also be seen on this plot. The increase in measured displacement with almost no change in load is believed to correspond to relative slip between the upper and lower main members. The measured load capacity of the specimen corresponding to net section fracture of the upper main member was 3.7% smaller than the capacity predicted based on the AISC procedure.

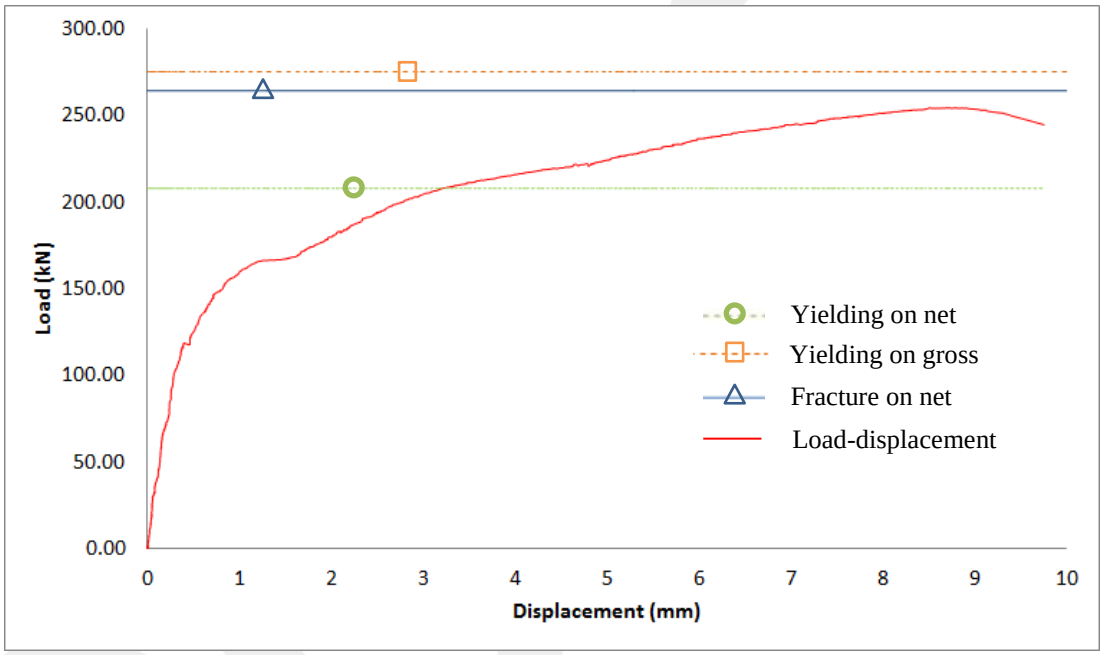

Figure 2.38. Load-displacement behavior for Specimen-2

Strain Gage Readings

Location of strain gages on the main members and interior reinforcement angle member are shown in Figures 2.39 and 2.40. Totally eight gages were attached on these members. Readings from these gages were used to determine the strain distribution on these members. Four strain gages, two on each member, were placed on the two lower main members in same horizontal line. This was applied to see load distribution which was expected to get equal strain values from two lower main members. The other four strain gages were attached on both legs of interior reinforcement angle member. This was done to obtain the strain distribution and compare it with Specimen-1.

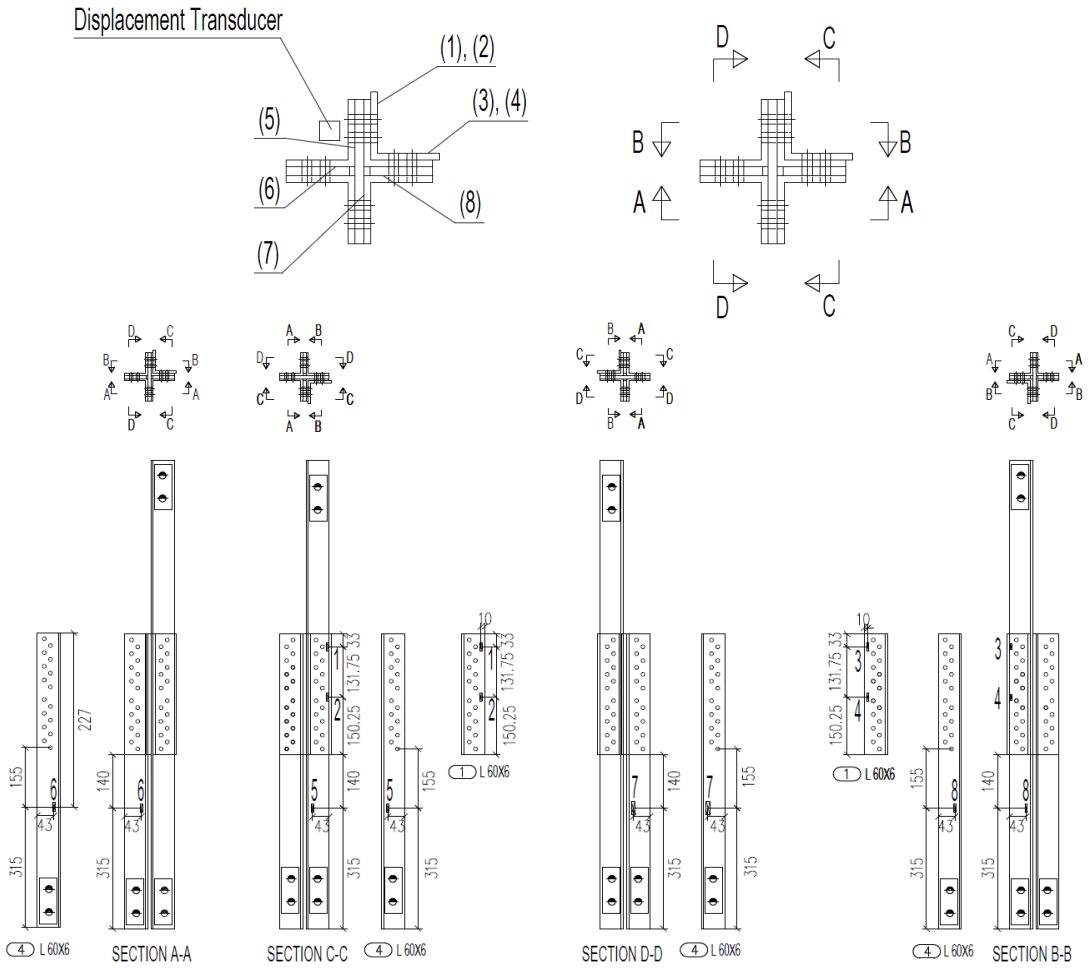

Figure 2.39. Strain gage and displacement transducer locations in side and cross-sectional view of Specimen-2 (dimensions in mm unit)

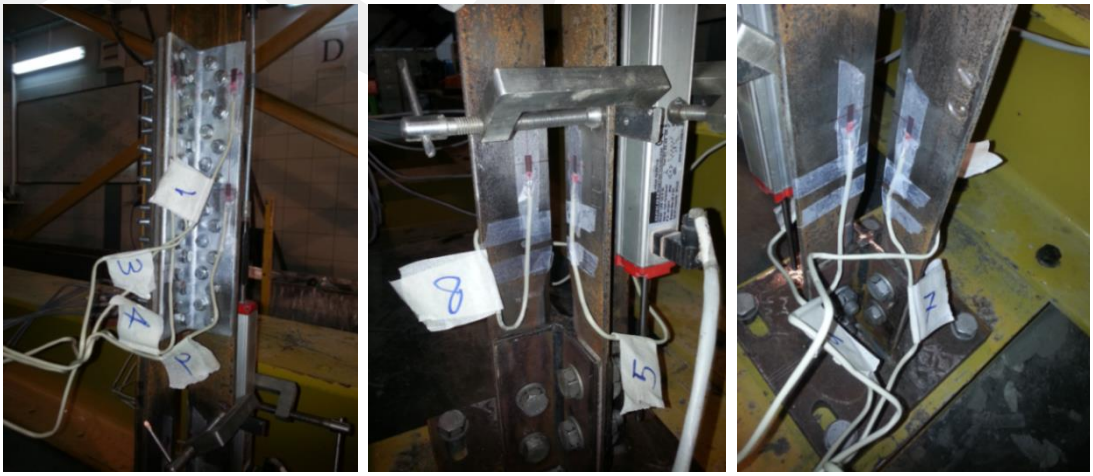

Figure 2.40. Members instrumented with strain gages (Specimen-2)

- **Strain Distribution in Interior Reinforcement Angle**

Data from strain gages located on the interior reinforcement angle (Gages 1-4) is given in Figure 2.41. These gages showed a similar behavior as in the previous specimen. Because of the presence of bending in addition to tensile axial force, both tensile and compressive strains were indicated by the gages.

Gages 1 and 3 were attached on the same horizontal line and on opposite legs of interior reinforcement angle. These gages were located on the upper part of the reinforcement angle member. These gages were expected to indicate similar strains. Partially similar behavior was observed. Gage 3 had higher strain values because of eccentricity. Because of the bending of upper main member, strains from Gage 1 were higher than those from Gage 3 to around 215.8 kN of loading. A similar behavior is observed between the readings of Gages 2 and 4. Strain profiles as indicated by Gages 1-4 under different load levels are shown in Figures 2.42 and 2.43.

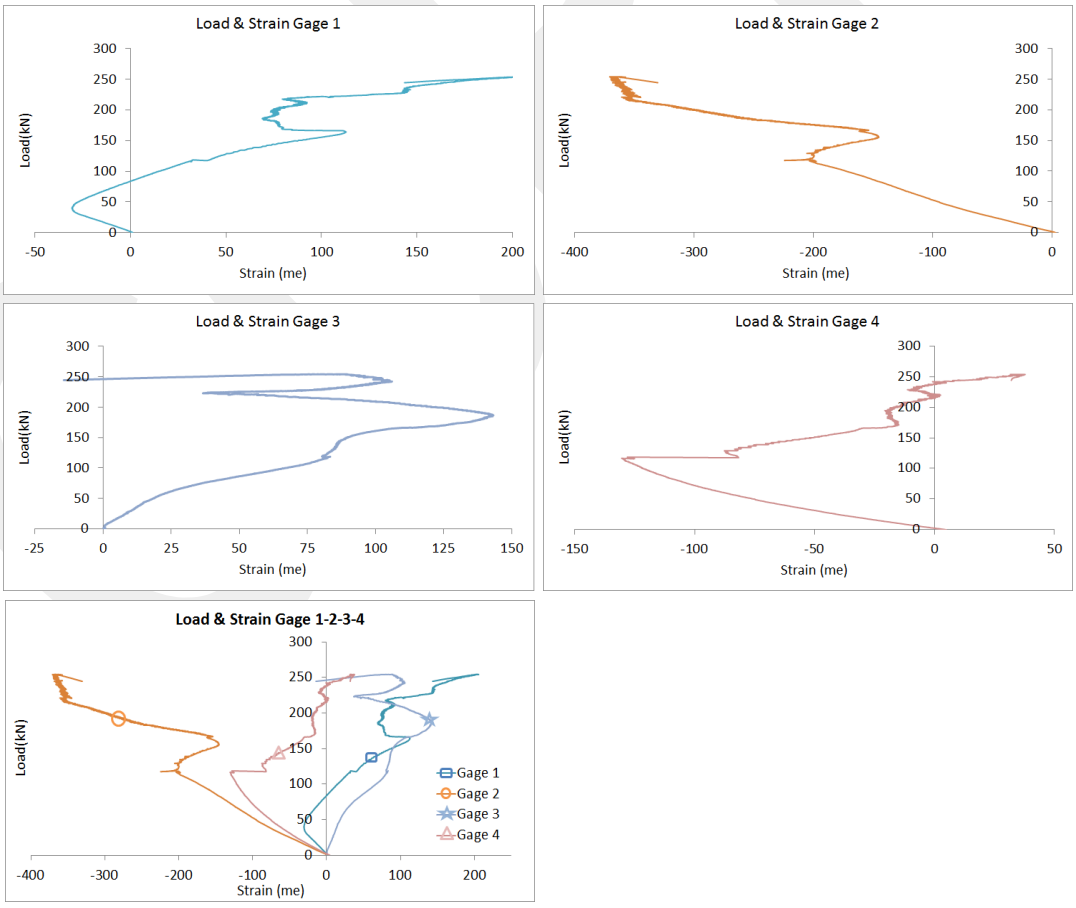

Figure 2.41. Strain distribution in interior reinforcement angle of Specimen-2

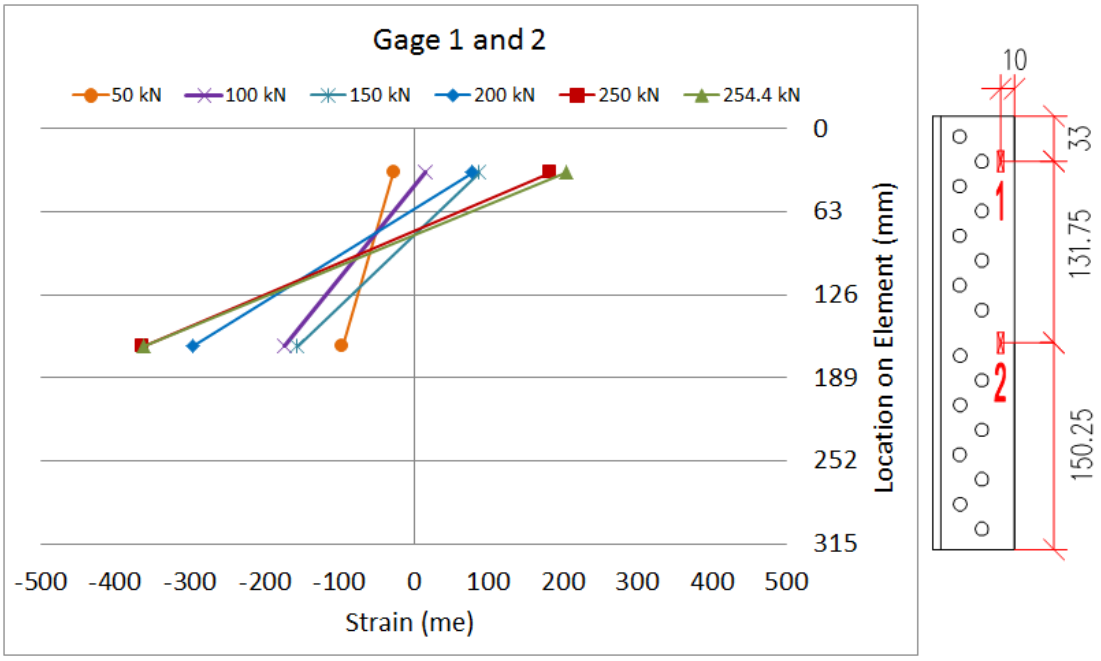

Figure 2.42. Variation of strain profile in interior reinforcement angle of Specimen-2 (dimensions in mm unit)

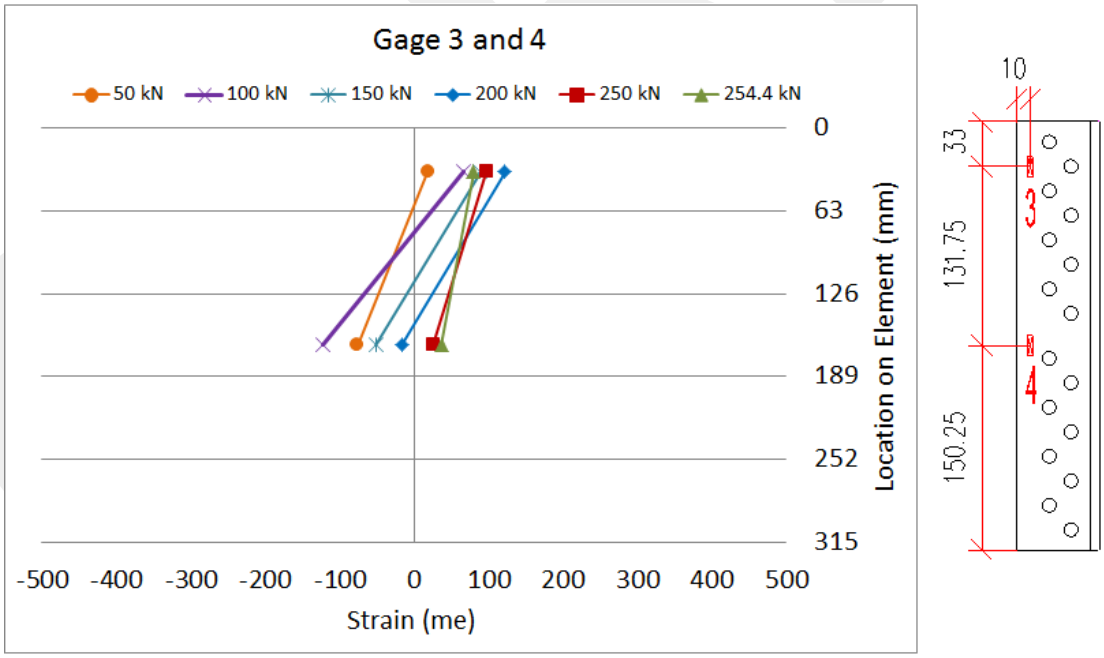

Figure 2.43. Variation of strain profile in interior reinforcement angle of Specimen-2 (dimensions in mm unit)

- **Strain Distribution in Lower Main Members**

Each one of Gages 5 and 8 were located on one of the lower main members. The fact that these two gages indicated very similar strain values is an indication that the total load is equally shared by the two lower main members. A similar agreement would be expected also between the readings of Gages 6 and 7. The small difference between the strains indicated by these gages could be attributed to additional bending of the main members under the applied load.

All gages include shear lag effect and bending. On the other hand, average strain line prepared as there is no shear lag and bending effect. In addition, it was thought that equal load distribution on two lower main members. As shown in Figure 2.44, Gage 6 and Gage 7 have lower strain values. Because, they are far away from the connection part. Also, Gage 5 and Gage 6 have higher strain values because of closer location to the connection part. Besides, strain values summation of four strain gages divided by four and it can be investigated.

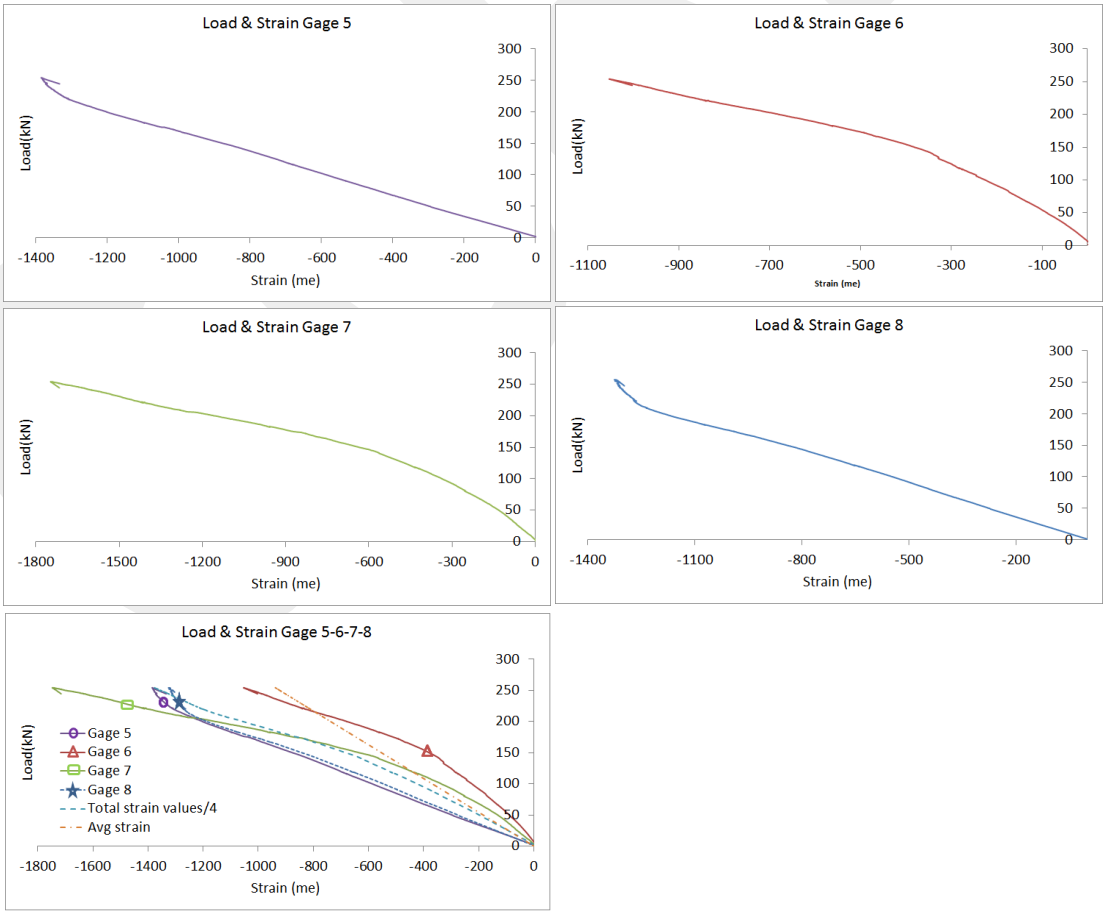

Figure 2.44. Strain distribution in lower main members of Specimen-2

2.2.4. Specimen-3

The connection detail used in Specimen-3 was identical to Specimen-2, except for the interior reinforcement angle. The interior reinforcement angle was eliminated in this specimen. The connection included sixty-four bolts in total. Used members, geometric details of the connection region in Specimen-3 and general views are given in Figures 2.45 and 2.46.

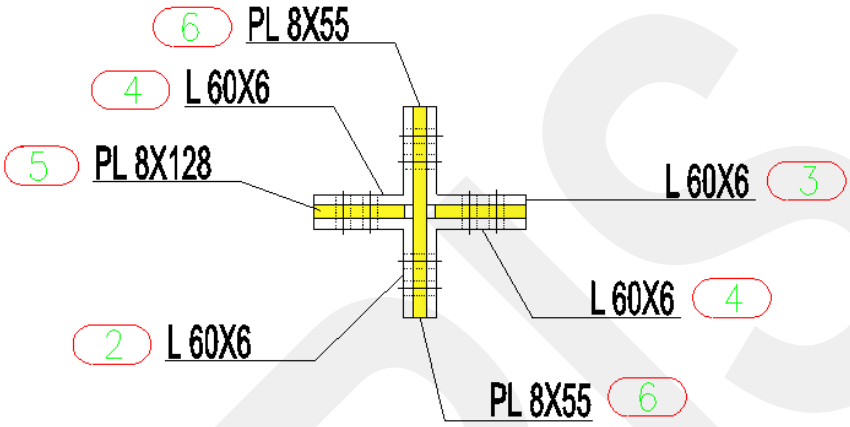

Figure 2.45. Cross-sectional view of Specimen-3

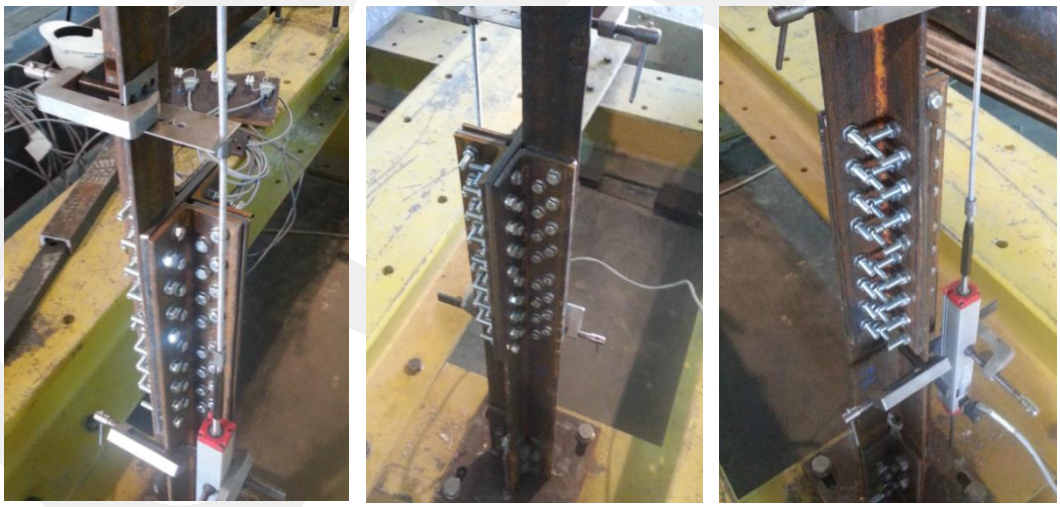

Figure 2.46. General view of Specimen-3

During the load testing of this specimen the upper main member was observed to undergo more significant bending deformation than the previous specimens (Figure 2.47). Based on this observation, it can be stated that interior reinforcement angle has a beneficial effect on reducing the bending deformation of the upper main member and this main member shows stiffer behavior with reinforcement angle.

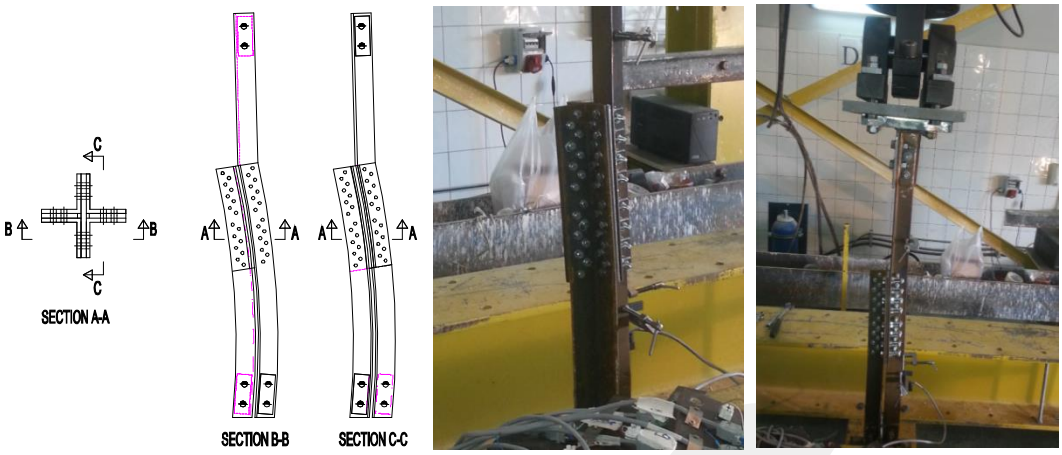

Figure 2.47. Deformed shape of Specimen-3

Predicted capacity corresponding to yielding on net section, fracture on net section, and yielding on gross section are calculated with average strength values of five specimens which were exposed to coupon tension test. Based on calculations, load capacity of the specimen corresponding to the failure mode of net section fracture was expected to be 259.3 kN. Failure of the specimen was actually the net section fracture of the upper main member at the first line of bolt with a maximum load of 257.6 kN. Therefore, the measured load capacity was 99.3% of the predicted capacity. The calculated capacity corresponding to yielding of the net section in the upper main member was 201 kN. The measured load-deflection response of the specimen together with the predicted capacities are shown in Figure 2.48.

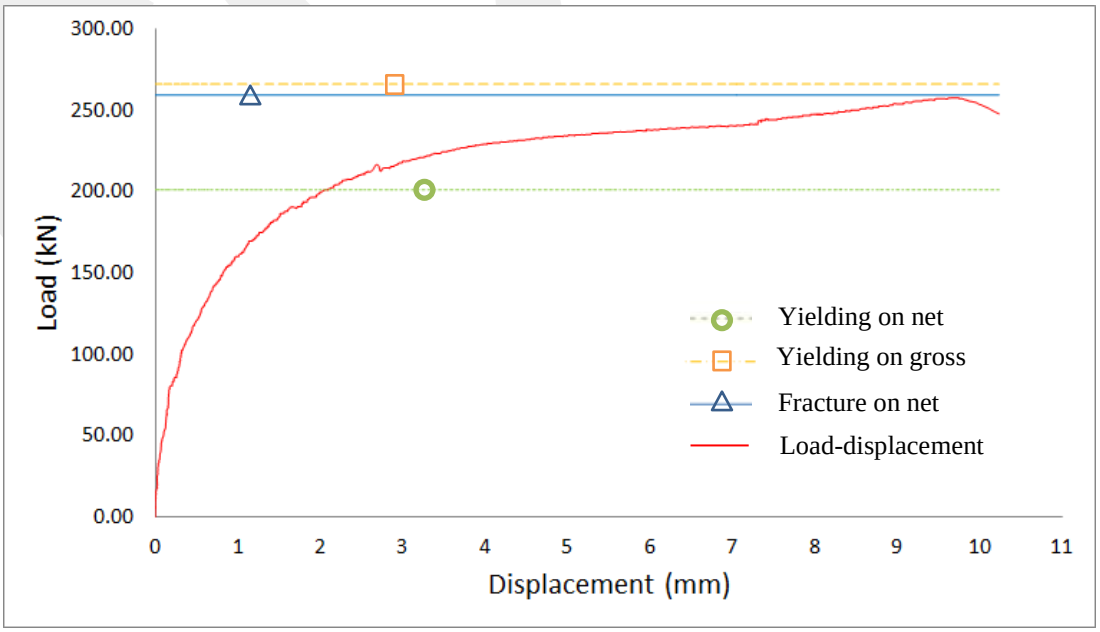

Figure 2.48. Load-displacement behavior for Specimen-3

Photographs of the fractured upper main member can be seen in Figures 2.49 and 2.50. Analysis of this member after the load test revealed necking of the member at the fracture section and bearing on the bolt holes, as seen on the photographs. Overall bending deformation of the member is also evident.

Figure 2.49. Rupture on critical path of Specimen-3

Figure 2.50. Bending of ruptured angle member of Specimen-3

Interior reinforcement angle member and filler plates were analysed and as shown in Figure 2.51, and no deformation was observed on these elements.

Figure 2.51. Reinforcement angle member and filler plates of Specimen-3, after testing

Bending on two lower main members together with a slight bearing deformation at bolt holes was also detected as in the previous specimens. These deformations are shown in Figures 2.52-2.53. In addition, bearing on critical path bolt holes can be seen in Figure 2.54.

Figure 2.52. Bending on lower main member 1 (Specimen-3)

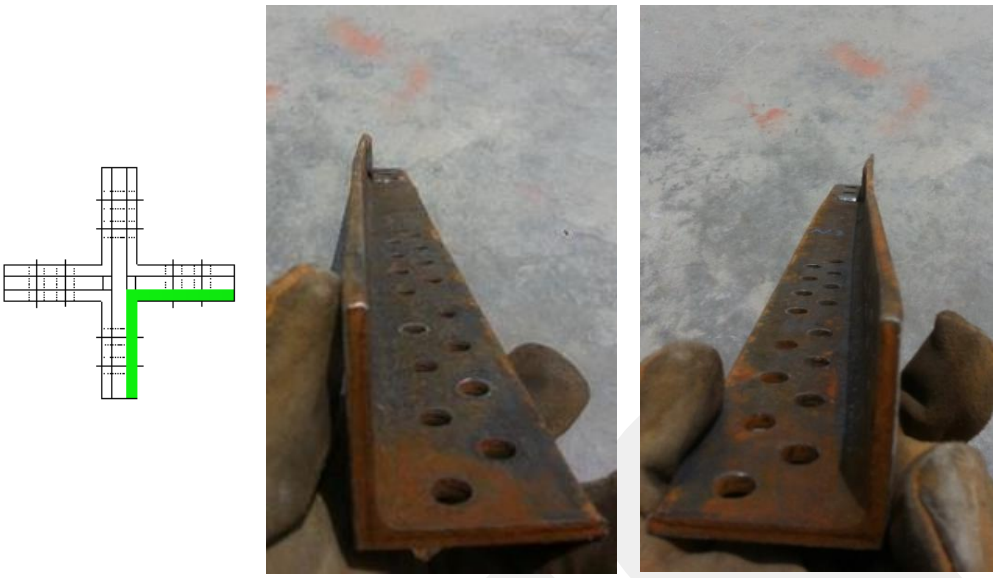

Figure 2.53. Bending on lower main member 2 (Specimen-3)

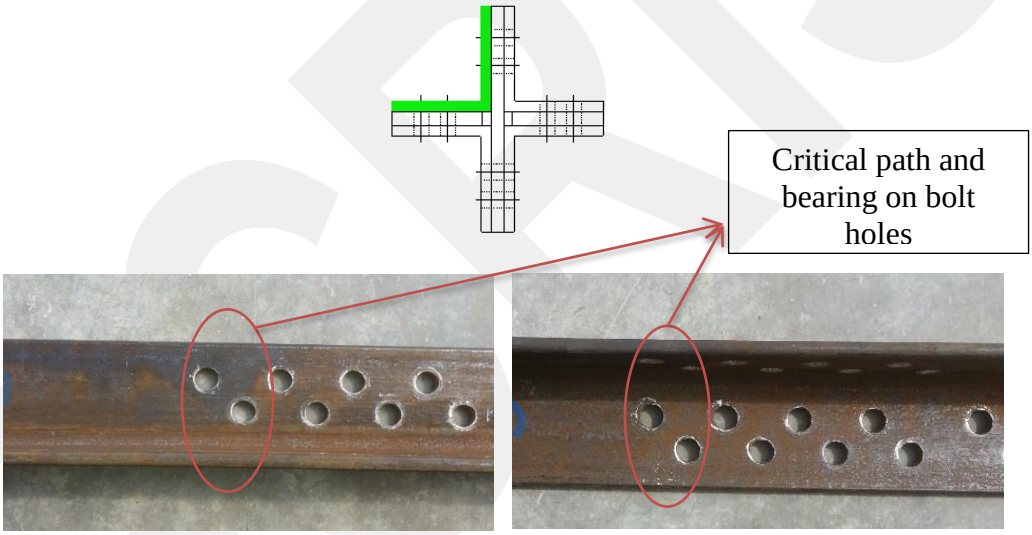

Figure 2.54. Bearing on lower main member 1 (Specimen-3)

2.2.5. Specimen-4

In the connection detail used in Specimen-4, no exterior reinforcement angle was used. The long filler plate between the lower main members was also eliminated, and a short piece of filler plate was provided between the upper main member and each of the lower main members. As a result of these modifications, the total number of bolts was reduced from sixty-four to thirty-two. Used members, geometric details of the connection region in Specimen-4 and general views are given in Figures 2.55 and 2.56.

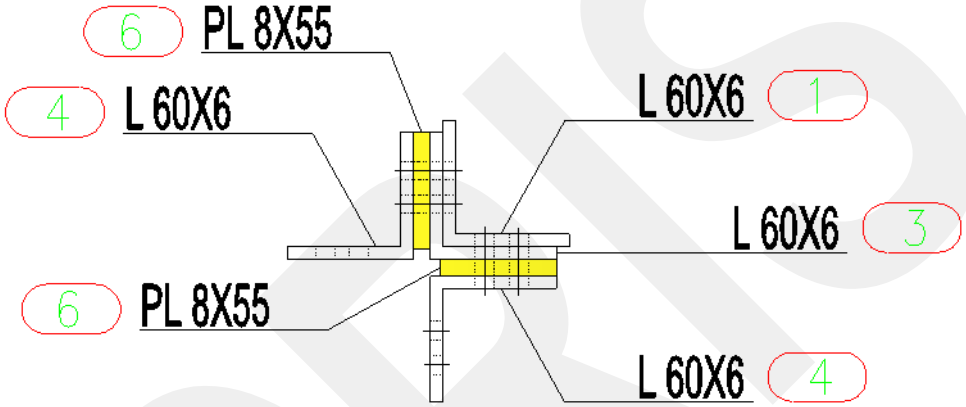

Figure 2.55. Cross-sectional view of Specimen-4

Figure 2.56. General view of Specimen-4

Failure of the specimen was fracture of the upper main member at first line of bolt with a maximum load of 270.3 kN (Figure 2.57). This level of capacity was very similar to the previous specimens, which included two times more bolts than this specimen. Therefore, this observation indicates that original connection detail was an overdesign in terms of the total number of bolts used to finish the connection. The measured load-deflection response of the specimen together with the predicted capacities are shown in Figure 2.58. The predicted capacity corresponding to net section fracture of the upper main member was 261 kN, which represents 96.6% of the measured capacity. The sudden increase of displacement at a load value of around 200 kN is an indication of a sudden relative slip between the upper and lower main members.

Figure 2.57. Rupture on critical path of Specimen-4

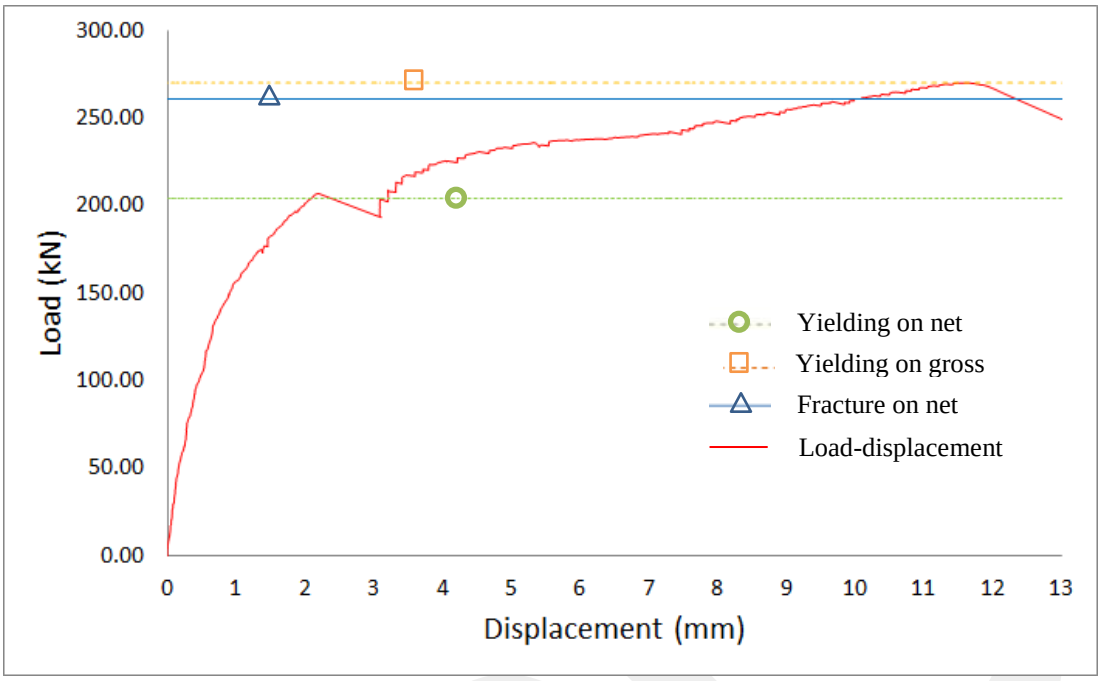

Figure 2.58. Load-displacement behavior for Specimen-4

Ruptured angle arm was analysed. Necking, bearing on bolt holes and bending can be seen in Figure 2.59. Bending on this arm was higher than the previous four specimens. Reinforcement angle members and filler plates were analysed and as shown in Figure 2.60, there was no deformation on those elements.

Figure 2.59. Bending of ruptured angle member of Specimen-4

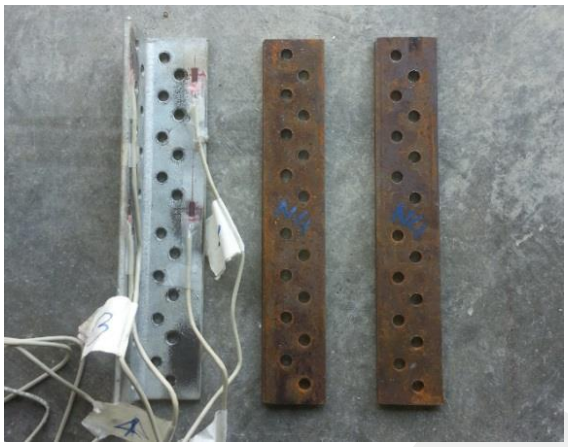

Figure 2.60. Reinforcement angle members and filler plates of Specimen-4, after testing

Behavior of lower main members was same as previous specimens in a sense that additional bending deformations occurred. Bending deformations were more significant for this specimen than the previously tested specimens, and this was attributed to the lack of long filler plate. In the previous specimens, the two main members were connected together by a long filler plate, and this was not the case with Specimen-4. This condition introduced additional "flexibility" and resulted in more significant bending deformation especially in the lower main members (Figures 2.61 and 2.62). Bearing deformations on the lower main members were observed to be somewhat less than the previous specimens (Figure 2.63).

Figure 2.61. Bending on lower main member 1 (Specimen-4)

Figure 2.62. Bending on lower main member 2 (Specimen-4)

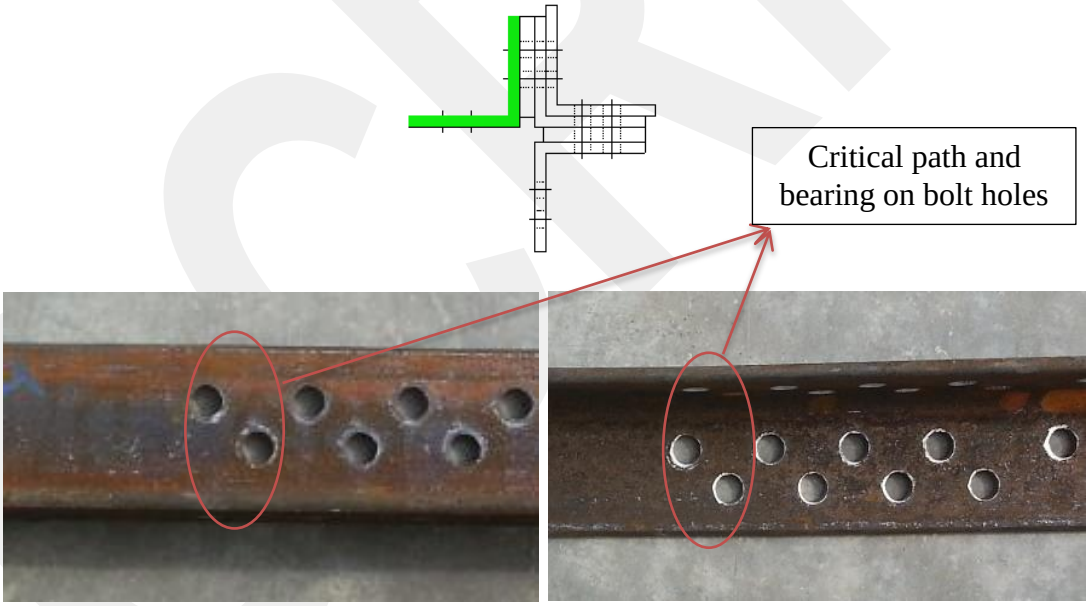

Figure 2.63. Bearing on lower main member 1 (Specimen-4)

Strain Gage Readings

The interior reinforcement angle member in Specimen-4 was instrumented with totally four strain gages, as shown is Figure 2.64 and 2.65. Location of these gages on the angle section was the same as in Specimen-2. With this orientation, Gages 1 and 3, and Gages 2 and 4 were expected to indicate similar strains. Plots shown in

Figure 2.66 indicate strains that are somewhat consistent with this expectation at relatively small load levels. Presence of compressive strains (at locations of Gages 1 and 3) also indicate additional bending deformation on the interior reinforcement angle. Strain profiles as indicated by Gages 1-4 under different load levels are shown in Figures 2.67 and 2.68.

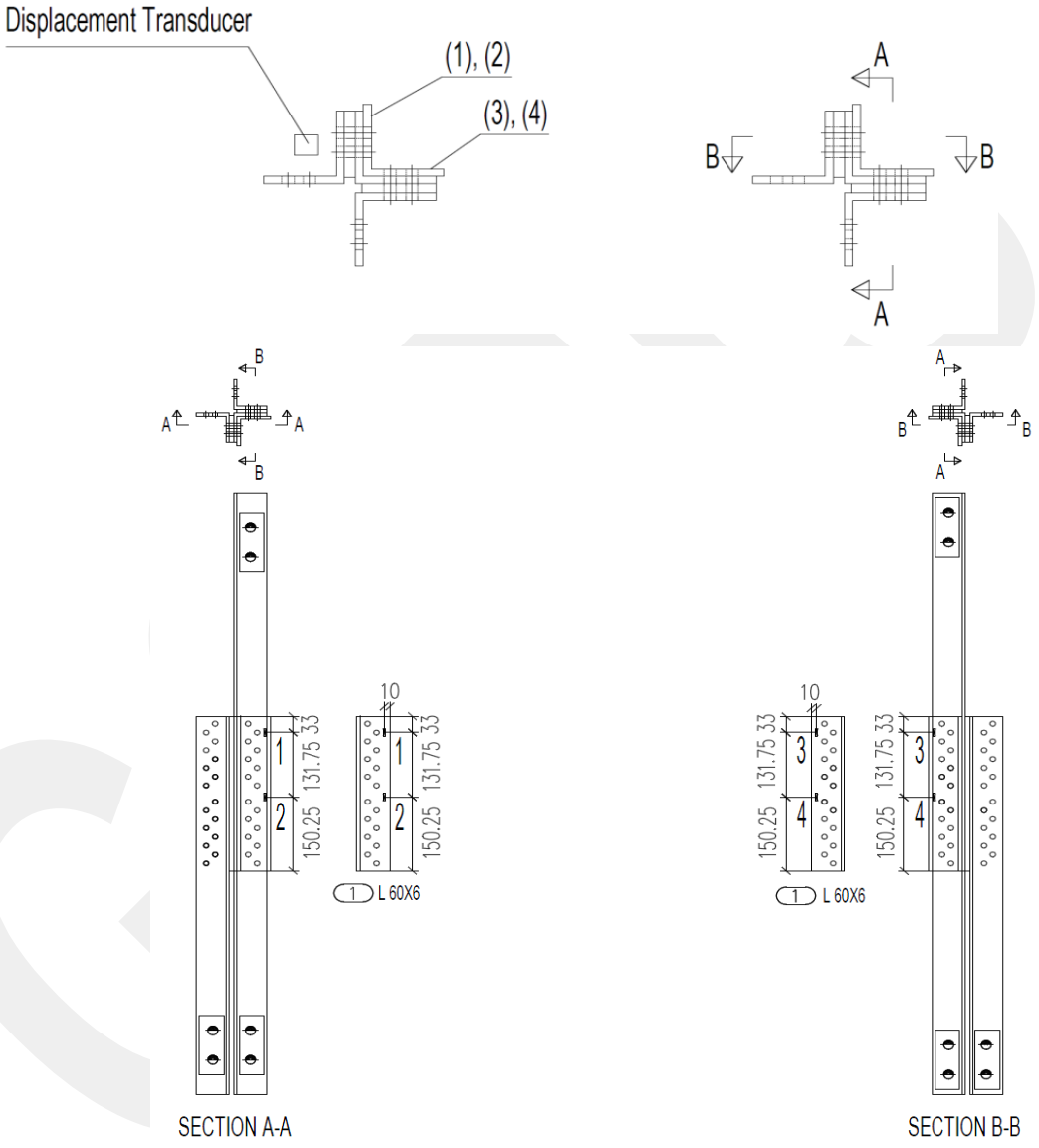

Figure 2.64. Strain gage and displacement transducer locations in side and cross-sectional view of Specimen-4 (dimensions in mm unit)

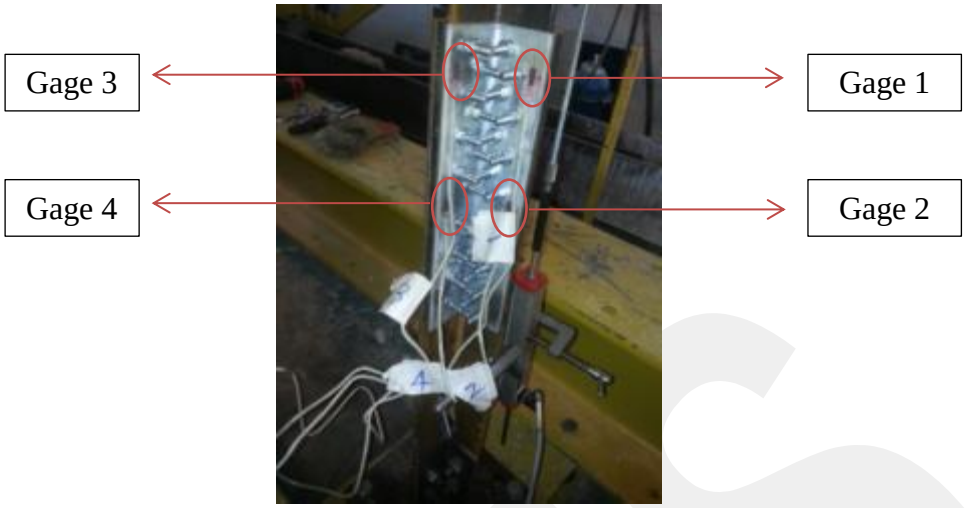

Figure 2.65. Strain gage numbers and locations (Specimen-4)

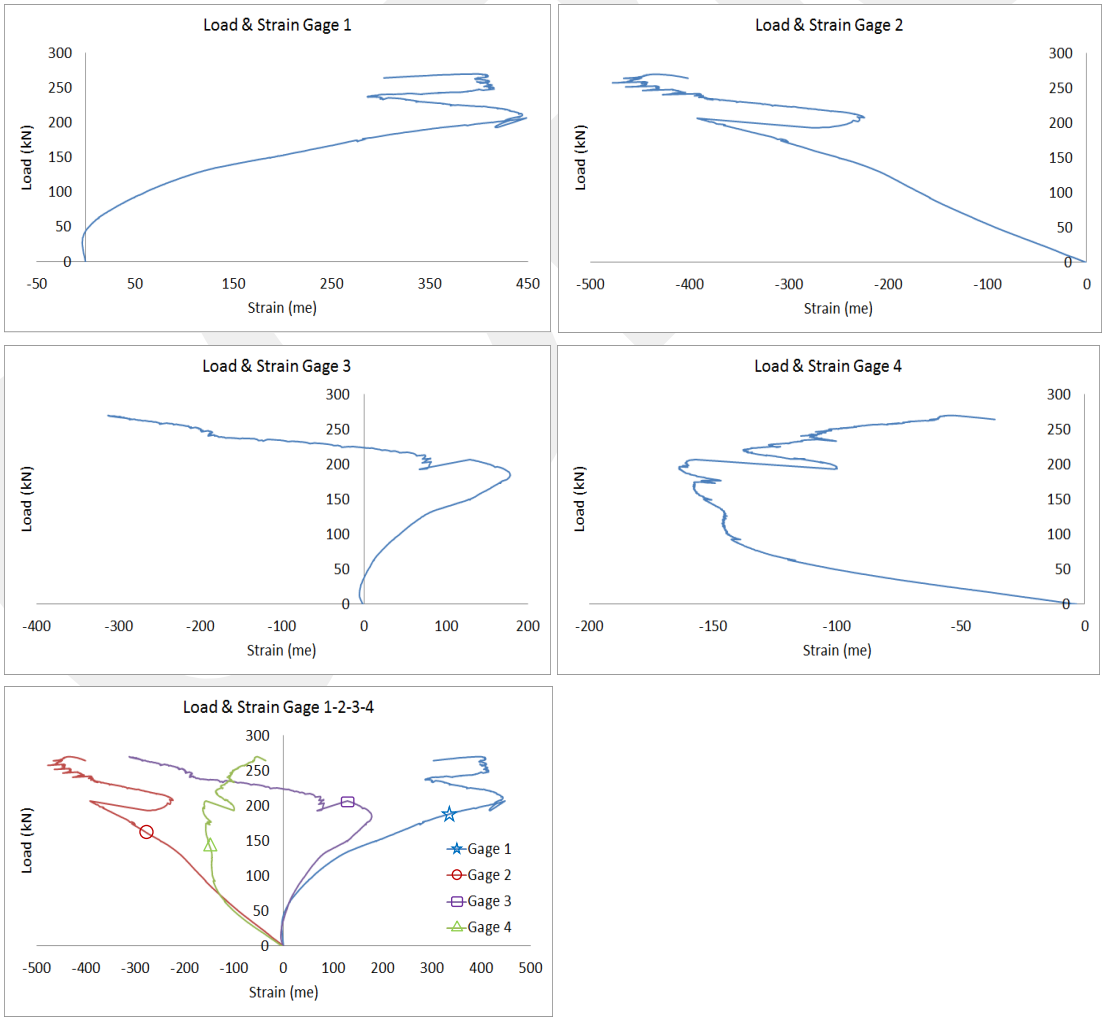

Figure 2.66. Strain distribution in interior reinforcement angle of Specimen-4

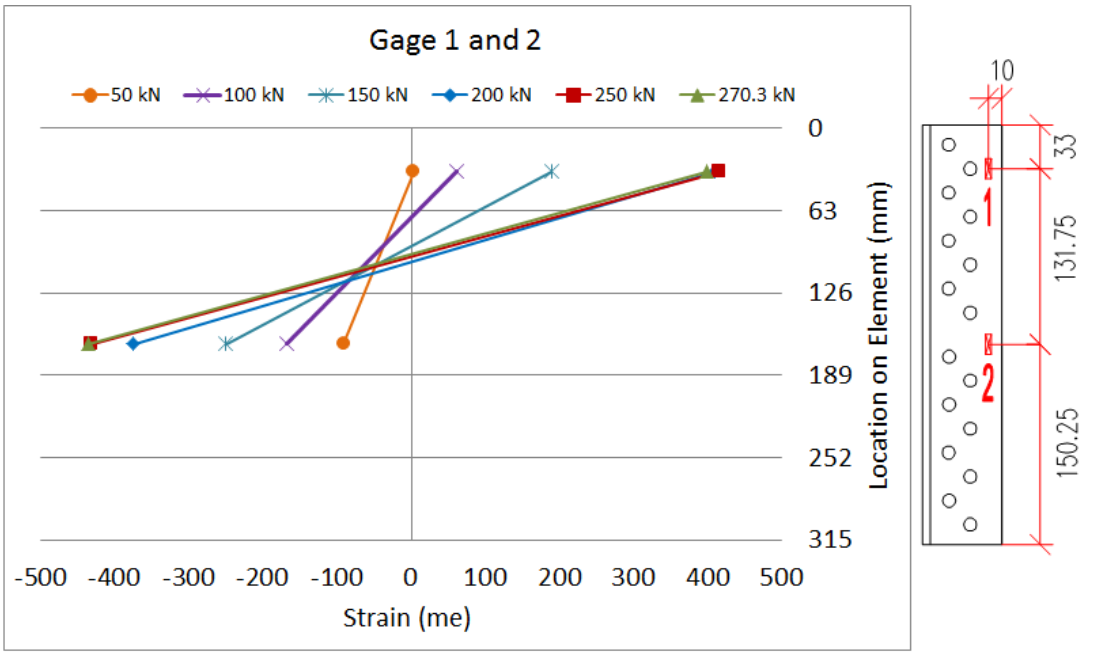

Figure 2.67. Variation of strain profile in upper main member of Specimen-4 (dimensions in mm unit)

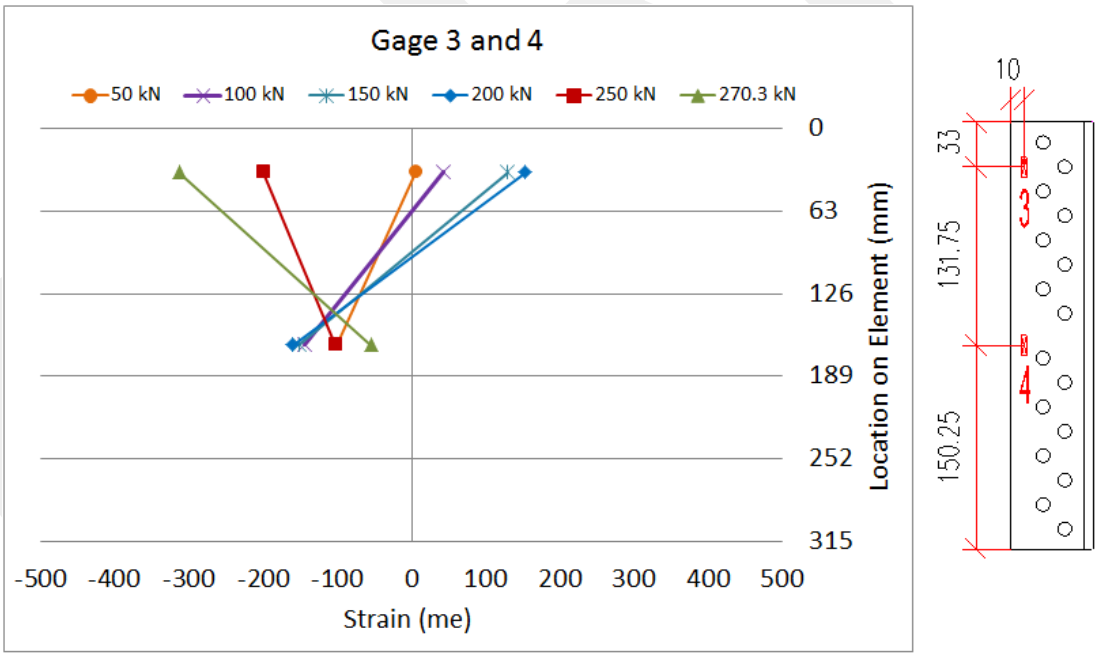

Figure 2.68. Variation of strain profile in upper main member of Specimen-4 (dimensions in mm unit)

2.2.6. Specimen-5

The connection detail used in Specimen-5 was similar to the one in Specimen-4. The only difference between these two details was that the interior reinforcement angle was eliminated in Specimen-5. Therefore this detail did not include the interior and exterior reinforcement angles, and represents the simplest connection geometry tested in the study. The total number of bolts used in the connection was still thirty-two. Used members, geometric details of the connection region in Specimen-5 and general views are given in Figures 2.69 and 2.70.

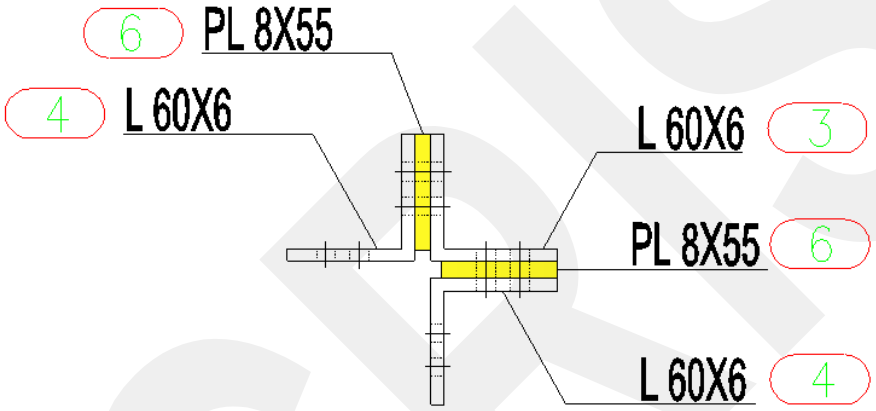

Figure 2.69. Cross-sectional view of Specimen-5

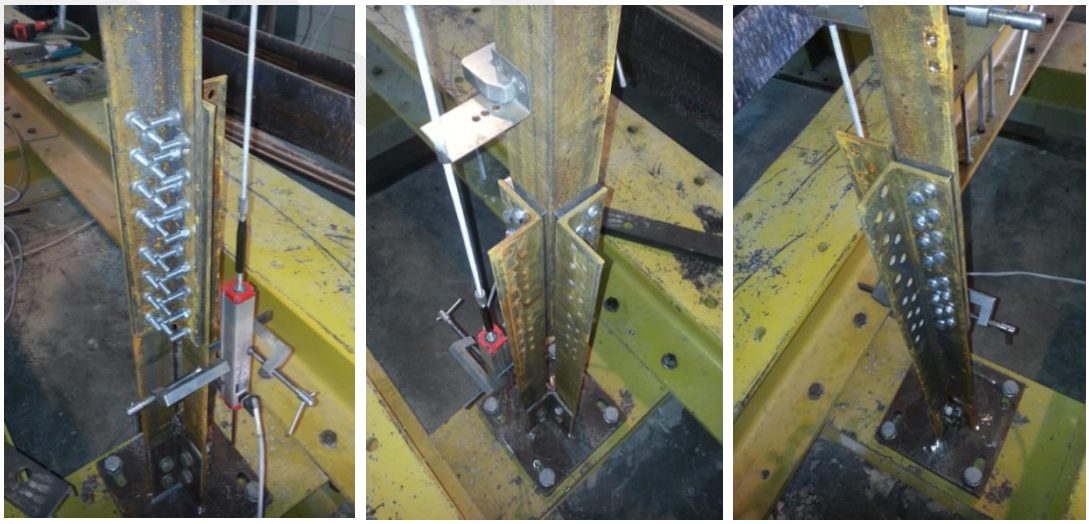

Figure 2.70. General view of Specimen-5

The specimen reached a maximum load of 269.6 kN, after which the upper main member underwent net section fracture (see Figure 2.71 to see ruptured upper main member). This measured maximum capacity corresponds to 106.9% of the predicted load capacity of 252.1 kN. The measured load-deflection response of the specimen is given in Figure 2.72. Similar to Specimen-4, the sudden increase of displacement at a load value of around 180 kN is believed to be an indication of a sudden relative slip between the upper and lower main members.

Figure 2.71. Rupture on critical path of Specimen-5

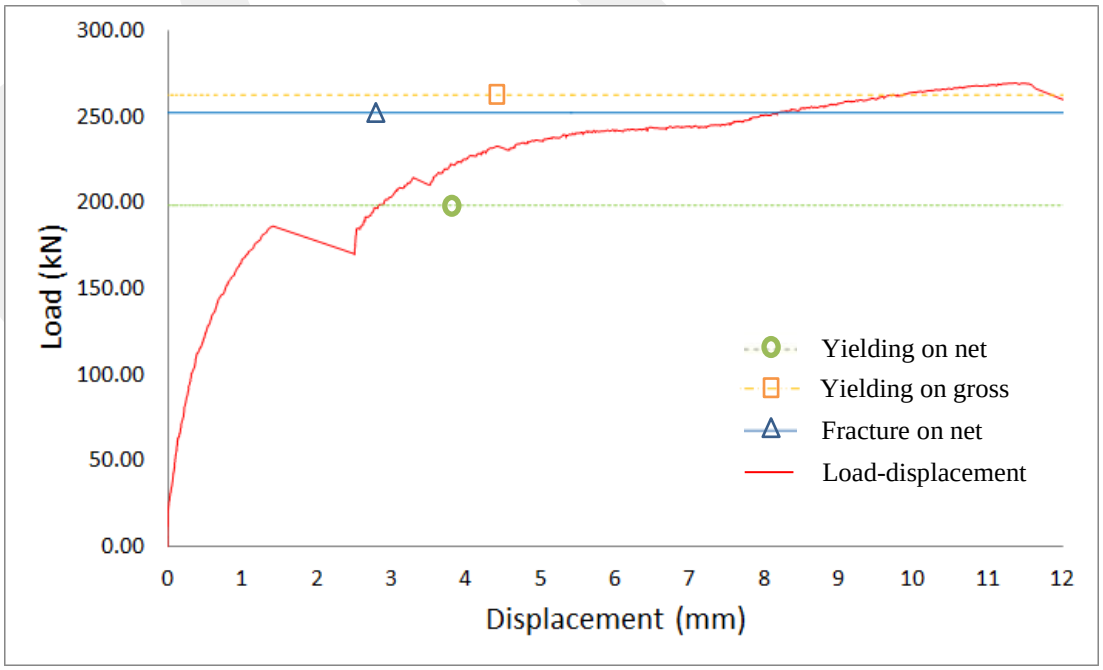

Figure 2.72. Load-displacement behavior for Specimen-5

Ruptured upper main member was analysed. Necking, bearing on bolt holes and bending can be seen easily in Figure 2.73. Upper main member in this specimen was observed to undergo bending deformation much more than the previously tested specimens. The reason for such behavior is attributed to the loss of “stiffness” as a result of the lack of reinforcement angles. Filler plates were analysed and as shown in Figure 2.74, there was no deformation on those elements. Minimal bending deformation was observed on the lower main members (Figures 2.75 and 2.76). No bearing deformation was visible on the lower main members (Figure 2.77). Different from the previous specimens, bearing deformations were observed in the upper main member at bolt holes located near the fracture path (Figure 2.78).

Figure 2.73. Bending of ruptured angle member of Specimen-5

Figure 2.74. Filler plates of Specimen-5, after testing

Figure 2.75. Bending on lower main member 1 (Specimen-5)

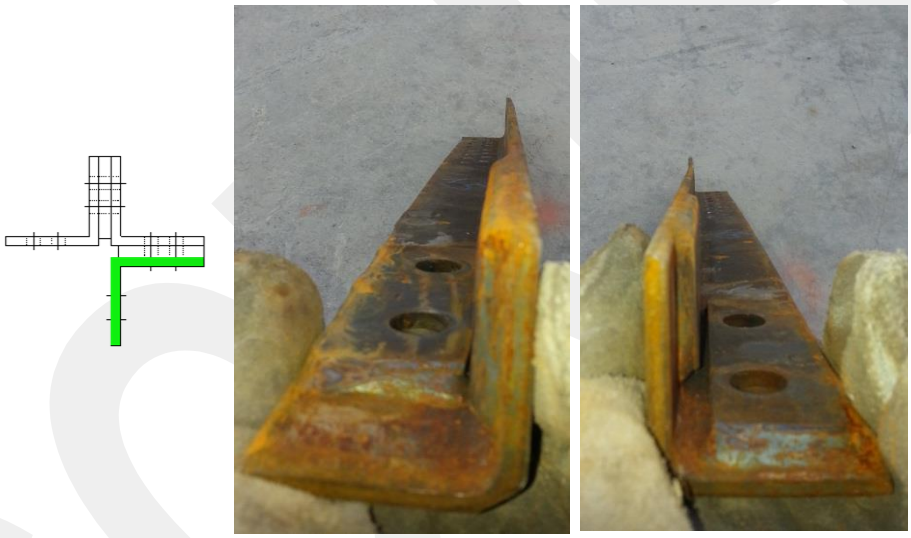

Figure 2.76. Bending on lower main member 2 (Specimen-5)

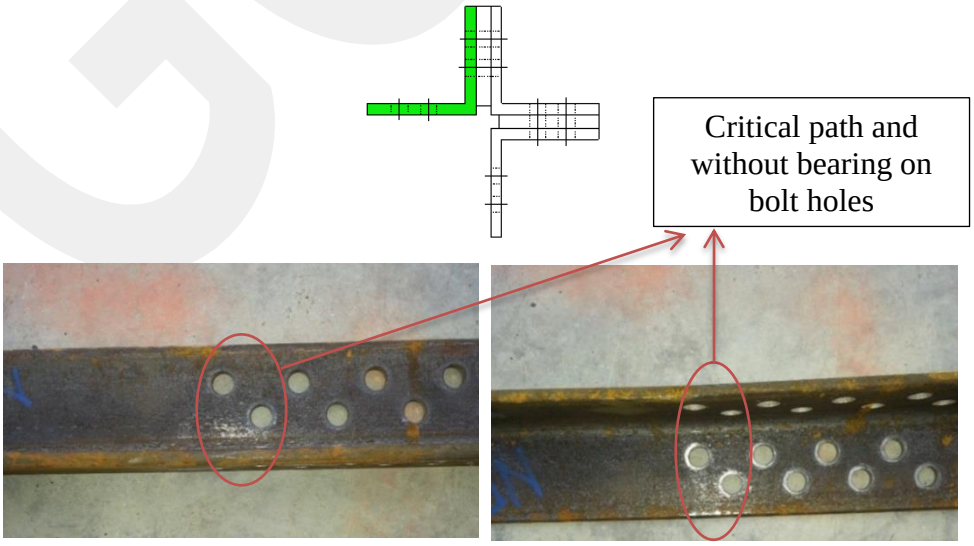

Figure 2.77. Bearing on lower main member 1 (Specimen-5)

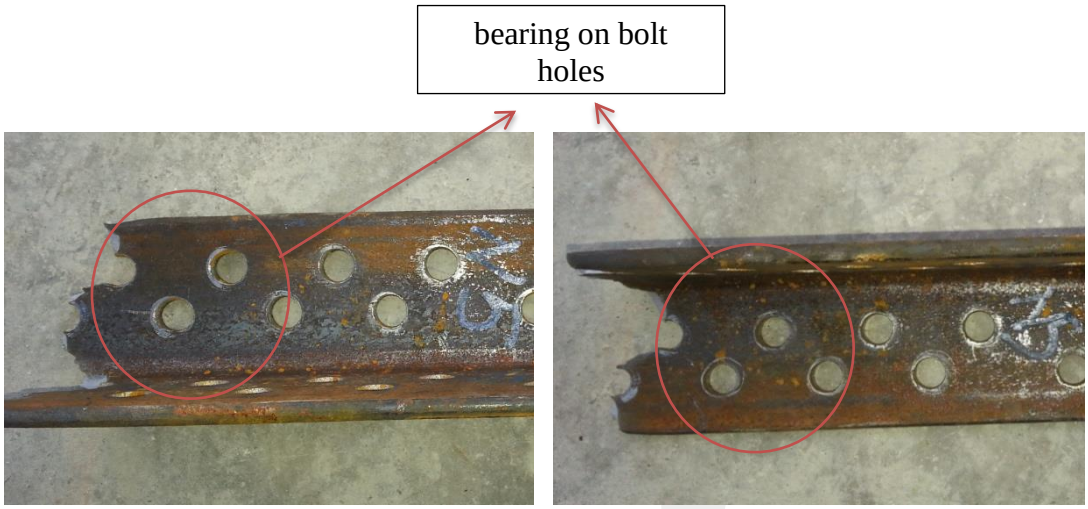

Figure 2.78. Bearing on upper main member (Specimen-5)

2.2.7. Specimen-6

One of the short filler plates in Specimen-5 was replaced by a long plate to connect the two lower main members together in Specimen-6 (Figures 2.79 and 2.80). This specimen did not have interior and exterior reinforcement angles, either, and included thirty-two bolts in total. Other than the absence of exterior reinforcement angle, this detail was also similar to the one used in Specimen-3.

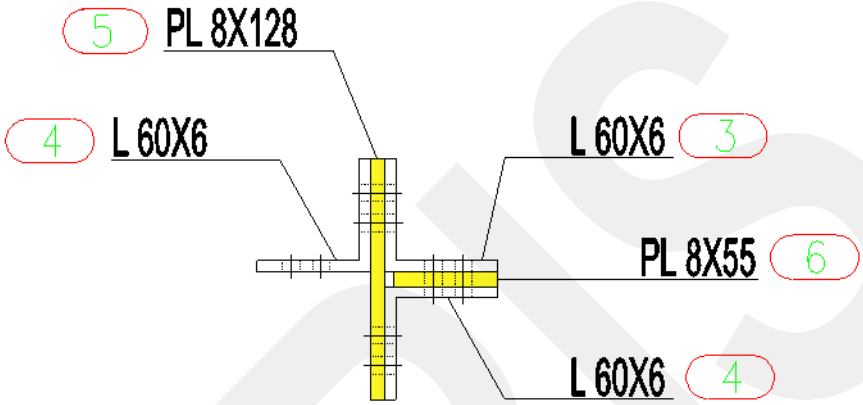

Figure 2.79. Cross-sectional view of Specimen-6

Figure 2.80. General view of Specimen-6

During the testing, bolts were observed to rotate in the direction of force and this rotation was visible with naked eye. Bolt rotations can be seen in Figure 2.81. After the testing bolts were analysed and bending deformation occurred on two of the bolts

that were located on the critical path. Bending deformation of these bolts can be seen in Figure 2.82.

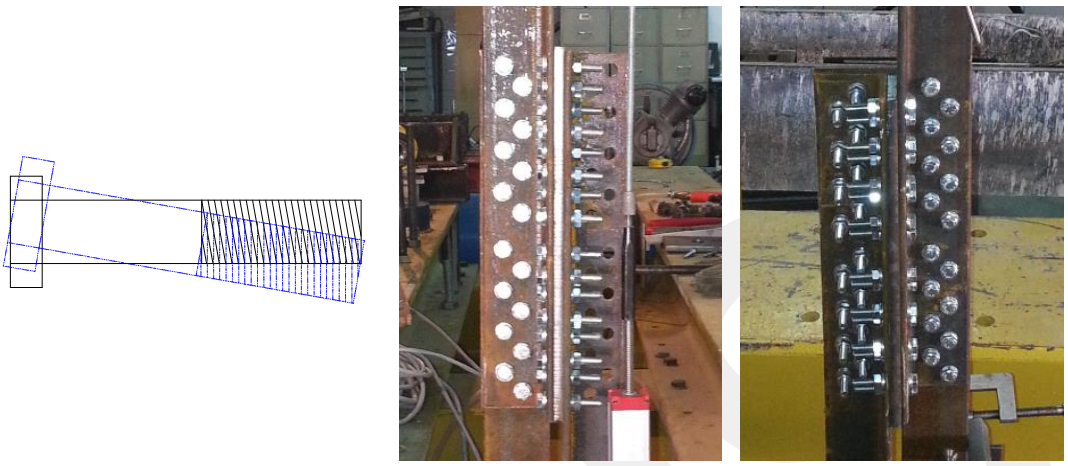

Figure 2.81. Rotation of bolts (Specimen-6)

Figure 2.82. Bending deformation on bolts (Specimen-6)

Fracture occurred on the upper main member (Figure 2.83) and the maximum load was 262 kN. The predicted load capacity corresponding to net section fracture of the upper main member was 245.3 kN. The measured load capacity corresponds to 106.8% of the predicted capacity. The measured load-deflection response of the specimen is given in Figure 2.84. A sudden relative slip between the upper and lower main members occurred under a load of approximately 130 kN.

Figure 2.83. Rupture on critical path of Specimen-6

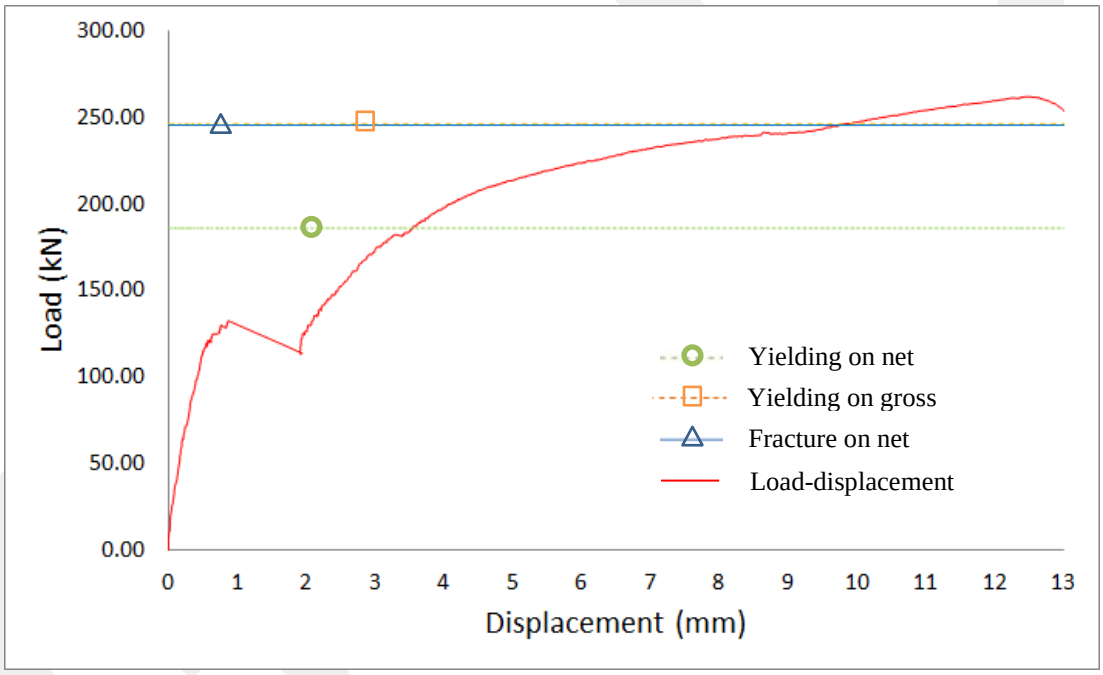

Figure 2.84. Load-displacement behavior for Specimen-6

Bending of the fractured upper main member is evident in the pictures given in Figure 2.85. Filler plates were analysed and as shown in Figure 2.86, there was no deformation on those elements. Bending deformations of lower main members can be seen in Figures 2.87 and 2.88. As shown in Figure 2.89, no bearing deformation was observed on the bolt holes at critical path. On the other hand, bearing deformations occurred in the upper main member at bolt holes located near the fracture path (Figure 2.90).

Figure 2.85. Bending of ruptured main member of Specimen-6

Figure 2.86. Filler plates of Specimen-6, after testing

Figure 2.87. Bending on lower main member 1 (Specimen-6)

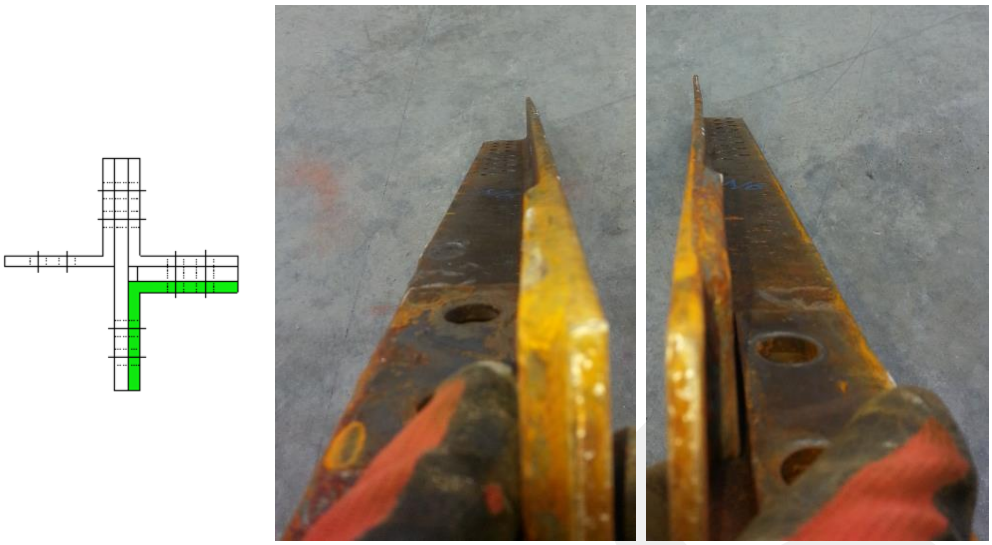

Figure 2.88. Bending on lower main member 2 (Specimen-6)

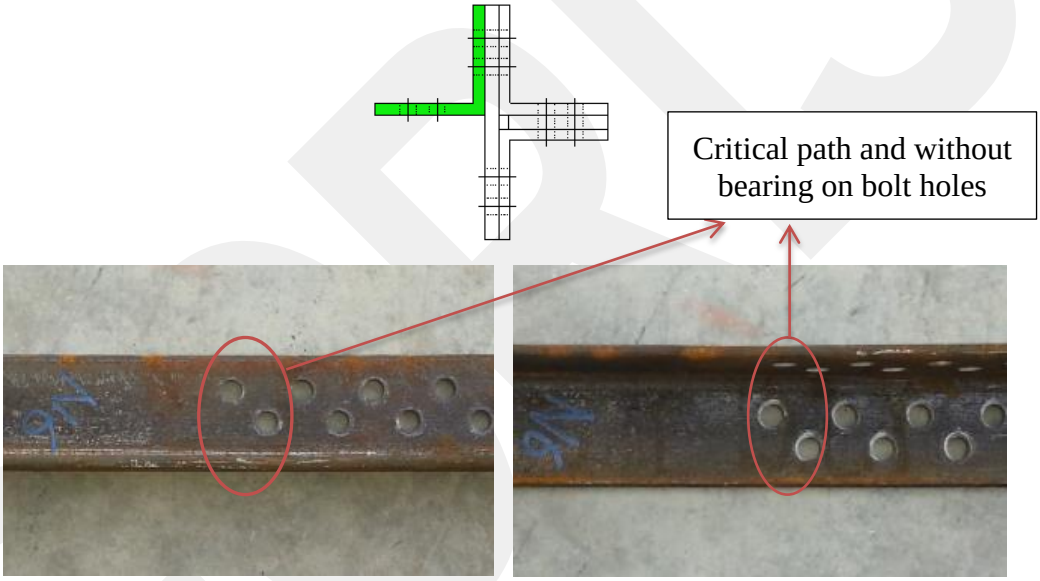

Figure 2.89. Bearing on lower main member 1 (Specimen-6)

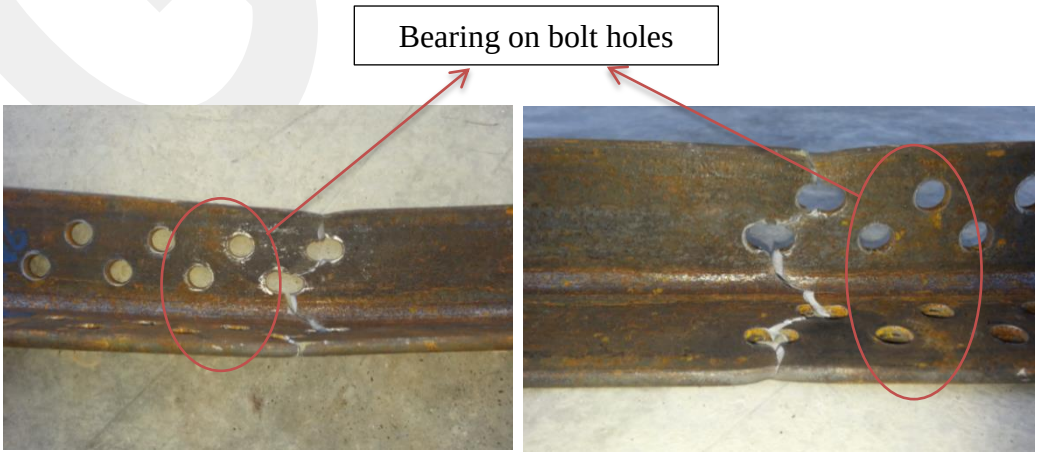

Figure 2.90. Bearing on upper main member (Specimen-6)

2.2.8. Specimen-7

The connection detail in Specimen-7 was identical to Specimen-5, except that the two regular filler plates were replaced by small pieces of washer plates. Two of these washer plates, one at the lower end of the connection and one at the upper end, were used instead of each of the regular filler plates. The total number of bolts used in the connection was still thirty-two. This detail, together with the one used in Specimen-5, represents the simplest connection geometry tested in the study. Geometric details of the connection region in Specimen-7 and general views are given in Figures 2.91 and 2.92.

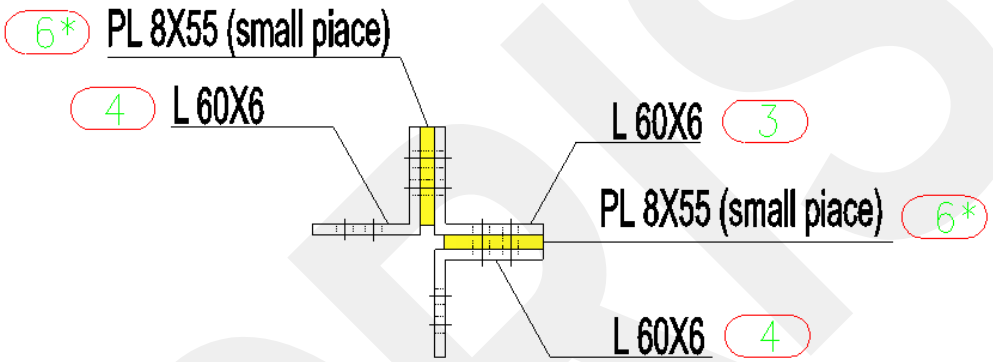

Figure 2.91. Cross-sectional view of Specimen-7

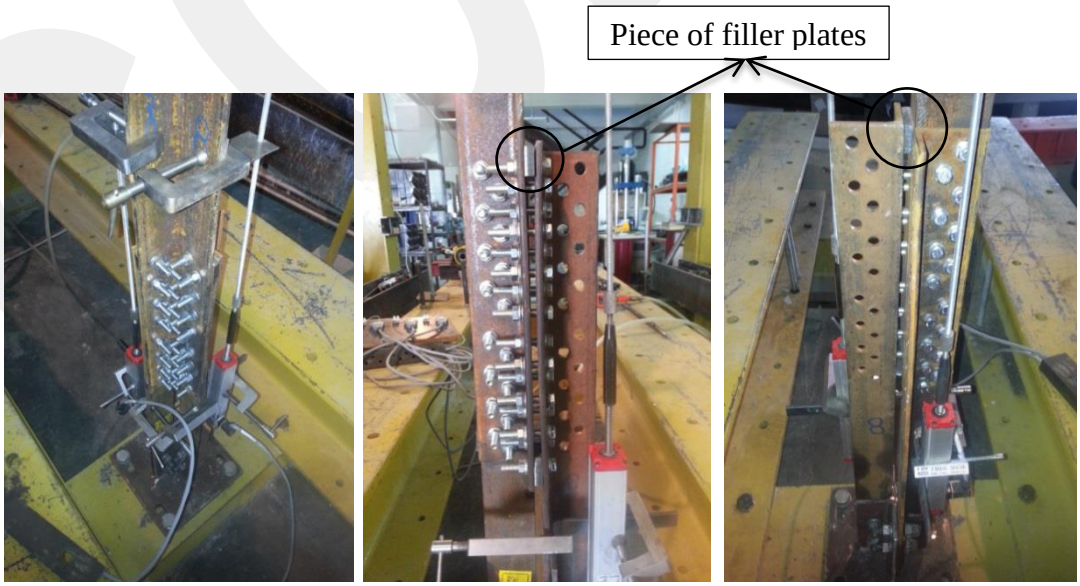

Figure 2.92. General view of Specimen-7

For this specimen, two displacement transducers were used to measure the deformation in the connection region. Readings from these two transducers were averaged to determine the displacement within the gage length used for the measurements. Locations of these displacement transducers can be seen in Figure 2.93.

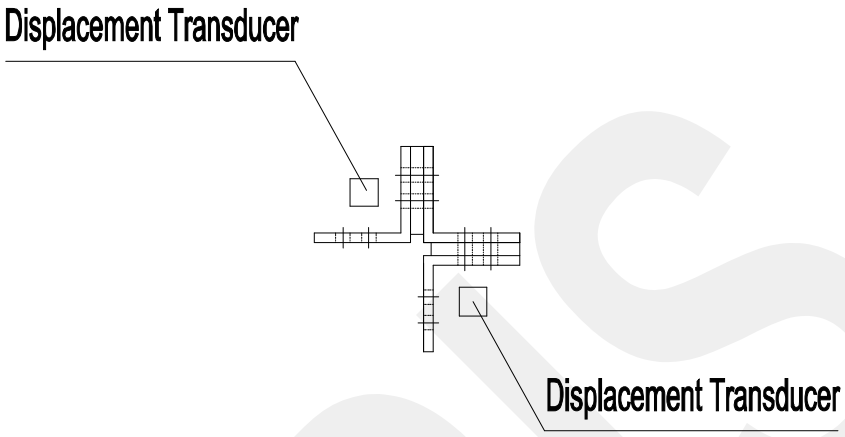

Figure 2.93. Displacement transducer locations in cross-sectional view (Specimen-7)

Specimen-7 behaved almost the same as Specimen-5, as expected. Different from Specimen-5, the bolts were observed to undergo significant amount of rotation during the laod test, as shown in Figure 2.94. The measured load capacity of the specimen was 272.5 kN, which correspond to 105.1% of the predicted capacity of 259.3 kN. Yielding on net section, fracture on net section, and yielding on gross section are calculated with average strain values as Specimen-3. Net section fracture occurred on the upper main member (Figure 2.95). The measured load-deflection response of the specimen is given in Figure 2.96.

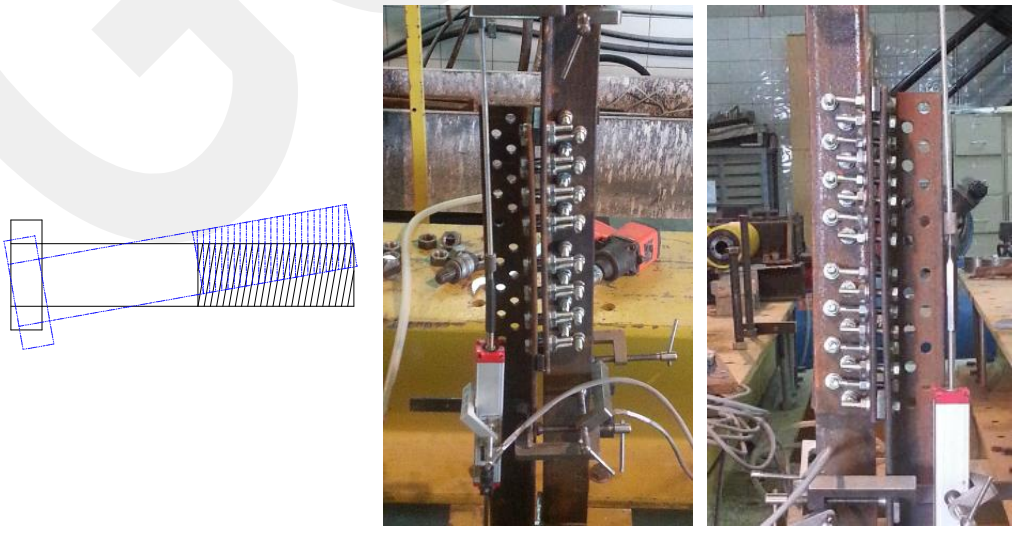

Figure 2.94. Rotation of bolts (Specimen-7)

Figure 2.95. Rupture on critical path of Specimen-7

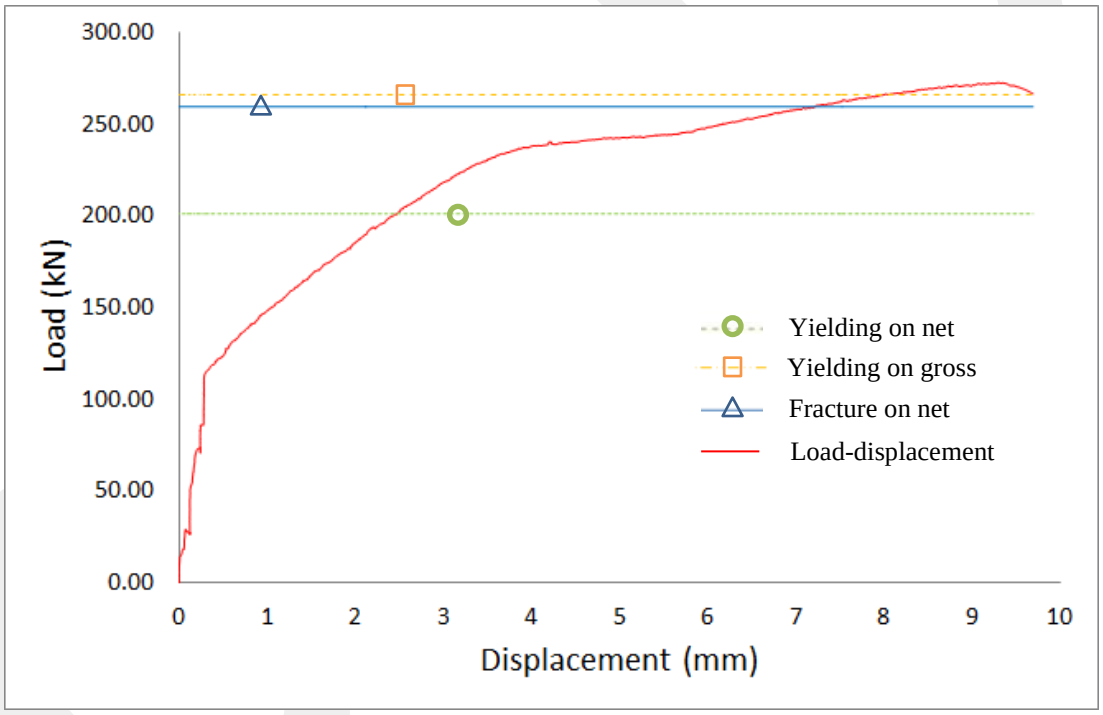

Figure 2.96. Load-displacement behavior for Specimen-7

Figure 2.97 shows the type and extent of deformations occurred on the upper main member. Similar to Specimen 5, significant amount of bending deformation occurred on the upper main member. The washer plates were analysed and as shown in Figure 2.98, there was no deformation on these elements. Bending deformation occurred on one of the lower main member is shown in Figure 2.99. Minor amount of bearing deformation was also observed around bolt holes at one leg of both of the lower main members (Figure 2.100).

Figure 2.97. Bending of ruptured main member of Specimen-7

Figure 2.98. Filler plates of Specimen-7, after testing

Figure 2.99. Bending on lower main member 2 (Specimen-7)

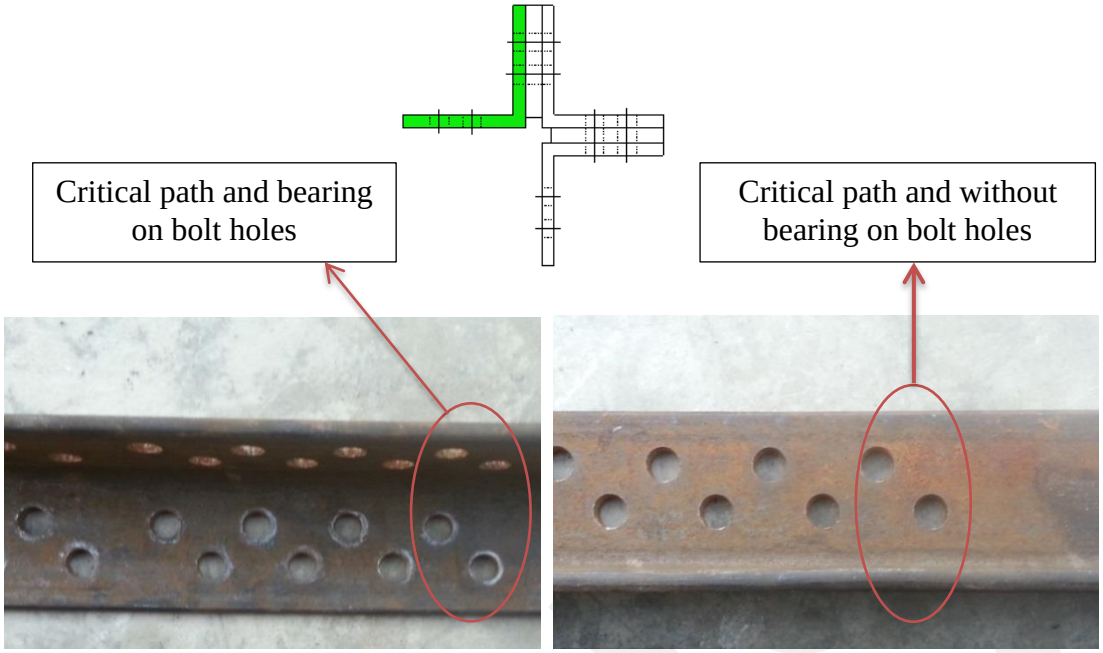

Figure 2.100. Bearing on lower main member 1 (Specimen-7)

2.3. COMPARISON OF THE BEHAVIOR OF CONNECTION DETAILS

A comparison of the load-displacement response of all six specimens with M8 type bolts is presented in Figure 3.101. All specimens exhibited similar response, which includes an initial linear behavior followed by a yielding portion and a secondary linear portion that continues until net section fracture of the upper main member.

The reason for having relative slip between the upper and lower main members only in some of the specimens was most likely the difference in the level of pretension in the bolts among the specimens. The bolts used in the specimens were tightened using an air impact wrench without any intent of applying pretension. Unintentional over-tightening of some of the bolts in some of the specimens, on the other hand, might have resulted in higher resistance against relative slip in these specimens than the other specimens. Any inaccurate configuration of bolt holes might have resulted in differences in the relative location of the holes in the upper and lower main members, which also might have affected the amount of relative slip. Therefore, if the slip evident in the load-displacement curves are ignored, then the difference between the curves would get even smaller.

Initial stiffness of specimens, as represented by the slope of the initial linear portion of load-displacement curve, was very similar. There were also very minor differences among the slope of the post-yield initial portion and the maximum load capacities. It should be noted here that the connection details in some of these specimens were much more complicated than the others, with twice the number of bolts. These major differences in the connection details did not cause any appreciable difference in the behavior of the specimens. From this perspective, it could be stated that the interior and exterior reinforcement angles and some of the filler plates used in the original connection detail could be eliminated and the number of bolts could be reduced by a half without a major change in the behavior of the connection under tensile loading.

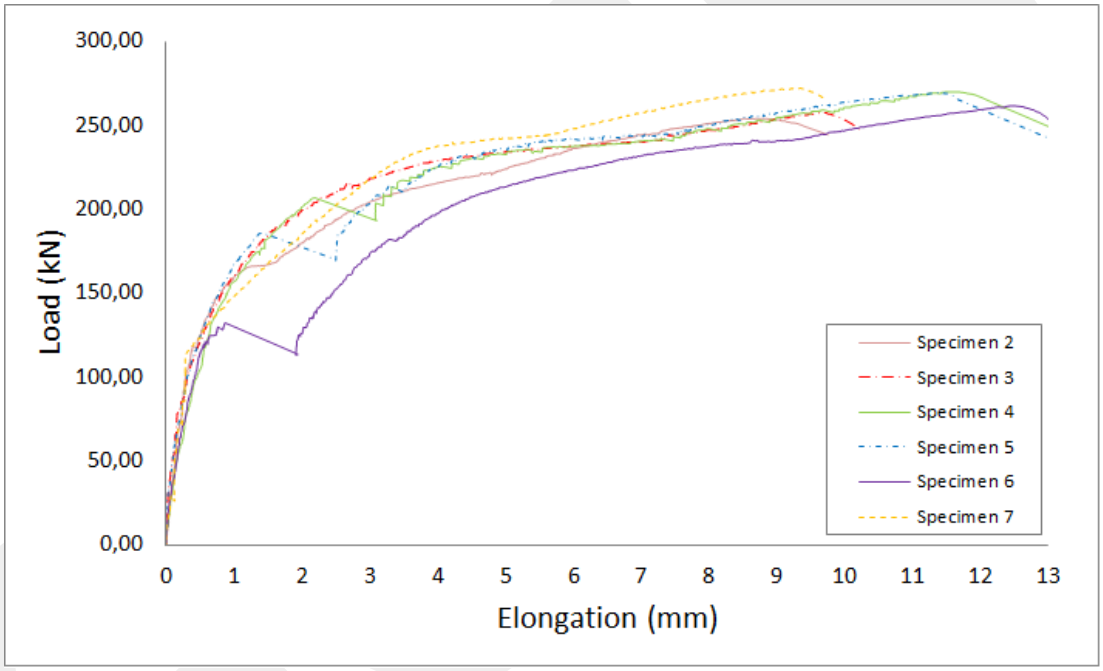

Figure 2.101. Load-displacement behavior comparison of all specimens

The measured load capacities of specimens are compared to the predicted capacities in Table 2.3. For each specimen, the predicted capacity corresponding to yielding on net section, fracture on net section, and yielding on gross section of the upper main member are provided.

As shown in Table 2.3, predicted fracture on net section and measured capacities are very close to each other. Some specimens have higher measured capacity according to predicted fracture on net section capacity and some specimens have lower

capacity. Measured capacity is expected higher than fracture on net section value to be safe side. Specimen-1 failed because of bolt failure, so it is not included with this issue. Specimen-2 and Specimen-3 are not providing this expectation for designing. Coupon tension test was not performed for Specimen-3 and average strength values of five specimens were used. Real yield and ultimate strength values of Specimen-3 could be higher and it could provide the expectation.

Table 2.3. Calculated and measured capacity results

	Predicted capacity (kN)			Measured capacity (kN)
	Y.O.N.[1]	F.O.N.[2]	Y.O.G.[3]	
Specimen 1	208.8	274.1	276.5	263.7 (bolt failure)
Specimen 2	207.8	264.1	275.0	254.4
Specimen 3	201.0	259.3	266.0	257.6
Specimen 4	204.1	261.0	270.2	270.3
Specimen 5	198.4	252.1	262.6	269.6
Specimen 6	185.8	245.3	246.0	262.0
Specimen 7	201.0	259.3	266.0	272.5

[1] Y.O.N.: yielding on net section

[2] F.O.N.: fracture on net section

[3] Y.O.G.: yielding on gross section

CHAPTER 3

CONCLUSIONS AND RECOMMENDATIONS

3.1. SUMMARY

The main objective of this study was to experimentally investigate the behavior of bolted splice connections of lattice overhead transmission line towers under tension loading. Seven specimens with each of them having a different connection detail were tested. All specimens were fabricated in production facility of Mitas Energy and Metal Construction Inc., and were tested at Atilim University Structural Mechanics Laboratory. The main parameters used in the testing program were the number of bolts used in the connection, presence of connection reinforcement angles, and the number and geometry of filler plates used between the main members. The connection details in some of these specimens were much more complicated than the others, with twice the number of bolts. Measured load capacity of the specimens was also compared with the predicted capacities calculated considering the applicable strength limit states. The study aimed at: (1) better understanding the load-flow mechanism in the connection, (2) determining the "redundant" members in the connection, and (3) simplifying the connection geometry by eliminating the redundant members

3.2. CONCLUSIONS

Following conclusions can be considered based on the results obtained during the experimental parts of the study;

- Major differences in the connection details did not cause any appreciable difference in the behavior of specimens. From this perspective, it could be stated that the interior and exterior reinforcement angles and some of the filler plates used in the original connection detail could be eliminated and the number of bolts could be reduced by a half without a major change in the behavior of the connection under tensile loading.
- The observed failure mode was bolt fracture on one specimen and net section fracture of the upper main member on the remaining six specimens. In all

specimens that had net section fracture of the upper main member, the fracture location was the same, and the maximum load resisted by these specimens were very similar.

- The measured load capacity of the specimens agreed well with the predicted load capacity corresponding to the failure mode of net section fracture of the upper main member. On the other hand, the predicted capacity corresponding to the limit state of net section yielding did not correspond to any physical deformation on the specimen.
- Strain measurements and observed deformation shapes indicate the presence of bending deformation of main members. This condition violates the pure axial tension member assumption used in the analysis and design stages of these latticed transmission towers. The reason for this bending deformation is the eccentricity between the line of application of the load and the centroidal axis of the angle members used for the main members.
- The detail used in Specimen-7 would result in a major saving in the material and workmanship costs over the currently used detail. Considering the case of only tensile loading, the currently used original detail can be replaced by this connection detail, because it produced similar load-deflection behavior and load capacity as the original connection detail.

3.3. RECOMMENDATIONS FOR FURTHER STUDY

The following recommendations can be made for future research;

- If a higher tensile load capacity is demanded, gross section of critical path can be increased by several methods. One of these methods could be to increase the cross-sectional are of the upper main member at the critical path by welding a reinforcement angle. Effectiveness of such methods can be studied by further research.
- This study is valid only for the case of tensile loading. Behavior of the same bolted splice connection under compressive loading needs to be investigated before providing recommendation for revision of this type of connections in actual overhead transmission line towers.

REFERENCES

[1] Fang, S.J., Roy, S. and Kramer, J.,1999, *Transmission Structures*, Structural Engineering Handbook.

[2] Barth, K.E., Orbison, J.G. and Nukala, R., 2002, *Behavior of Steel Tension Members Subjected to Uniaxial Loading*. Journal of Construction Steel Research, Vol. 58, 1103-1120.

[3] Zhuge, Y., Mills, J.E. and Ma X., 2012, *Modelling of Steel Lattice Tower Angle Legs Reinforced for Increased Load Capacity*. Engineering Structures, Vol. 43, 160-168.

[4] Puthli, R. and Fleischer, O., 2001, *Investigation on Bolted Connections for High Strength Steel Members.* Journal of Constructional Steel Research, Vol. 57, 313-326.

[5] Xie, Q. and Sun, L., 2013, *Experimental Study on the Mechanical Behavior and Failure Mechanism of a Latticed Steel Transmission Tower.* American Society of Civil Engineers, doi: 10.1061/(ASCE)ST.1943-541X.0000722.

[6] Salih, E.L., Gardner, L. and Nethercot, D.A., 2013, *Numerical Study of Stainless Steel Gusset Plate Connections.* Engineering Structures, Vol. 49, 448-464.

[7] Lu, C., Ma, X. and Mills, J.E., 2014, *The Structural Effect of Bolted Splices on Retrofitted Transmission Tower Angle Members*. Journal of Constructional Steel Research, Vol. 95, 263-278.

[8] Chesson, E.JR. and Munse, W.H., 1959, *Behavior of Large Riveted and Bolted Structural Connections*. Civil Engineering Studies/Structural Research Series, No.174.

[9] American Institute of Steel Construction (AISC), 2010, *Specification for Structural Steel Buildings*, ANSI/AISC 360-10.

APPENDIX A

SPECIMEN DESIGN CALCULATIONS

A.1. Scaling of the Prototype Design

The prototype tower had main leg members made of L160x17 angle section. Because load capacity of the testing frame used in this study was limited to nearly 400 kN, L160x17 angle section could not be used in the specimens. Because of this reason, the prototype design was scaled down according to the capacity of testing machine. L60x6 angle section was used in the specimens. This section has nearly the same width-to thickness ratio as the original L160x17 angle section.

Main member in prototype tower: L 160x17;

Member area = 51.80 cm^2

$\frac{L}{t} = \frac{160}{17} = 9.41$

Used Members in test specimens: L 60x6;

Member area = 6.91 cm^2

$\frac{L}{t} = \frac{60}{6} = 10$

Scale ratio = $\frac{51.8\ cm^2}{6.91\ cm^2} = 7.5 \quad \rightarrow \quad {}^{1}/_{7.5}$ scale

Grade of steel = S355 $\rightarrow$ f_y = 400 MPa = 400.000 kN/m^2

f_u = 525 MPa = 525.000 kN/m^2

Grade of bolts = 8.8 $\rightarrow$ f_y = 640 MPa = 640.000 kN/m2

f_u = 800 MPa = 800.000 kN/m2

A.1.1. Scaled Member Bolt Size

Bolts in prototype tower: 16 M20 $\rightarrow$ $A_{b,\,M20}$ = 3.14 cm^2 $\rightarrow$ Total $A_{b,\,M20}$ = 50.24 cm^2

16 M16 $\rightarrow$ $A_{b,\,M16}$ = 2.01 cm^2 $\rightarrow$ Total $A_{b,\,M16}$ = 32.16 cm^2

Total A_b = 82.4 cm^2

Scale $\rightarrow \frac{82.4\ cm^2}{7.5} = 10.99\ cm^2$

$\frac{10.99\ cm^2}{32\ bolts}$ = 0.34 cm^2 (Area of a single bolt)

$\frac{\pi D^2}{4}$= 0.34 cm^2 → D = 0.7 cm (not considering the reduction in bolt diameter due to threads)

Thread area=0.34 / 0.75 = 0.45 cm2 → D = 0.8 cm

* Use 32 M8 bolts (considering the reduction in bolt diameter due to threads)

A.1.2. Bolt Distances

According to AISC – Table J3.4M, bolt spacing and edge distance dimensions should be as below;

TABLE A.1. Part of table J 3.4M from AISC [9]

Bolt Diameter Ø(mm)	Sheared Edges – Le (mm)	Rolled Edges – Le′ (mm)
7	15*	13*
16	28	22
20	34	26

* Values were obtained with interpolation between M8 and M16 bolts

Sheared Edges (Le) = 15 mm (Interpolation) Le → 15 mm ≥ 15 mm √ O.K.

Rolled Edges (Le′) = 13 mm (Interpolation) Le′→ 18 mm ≥ 13 mm √ O.K.

Bolt distances (3D) = 21 mm d → 24.1mm ≥ 21 mm √ O.K.

s = 18 mm

g= 16 mm

Minimum connection length of L60x6 = 315 mm

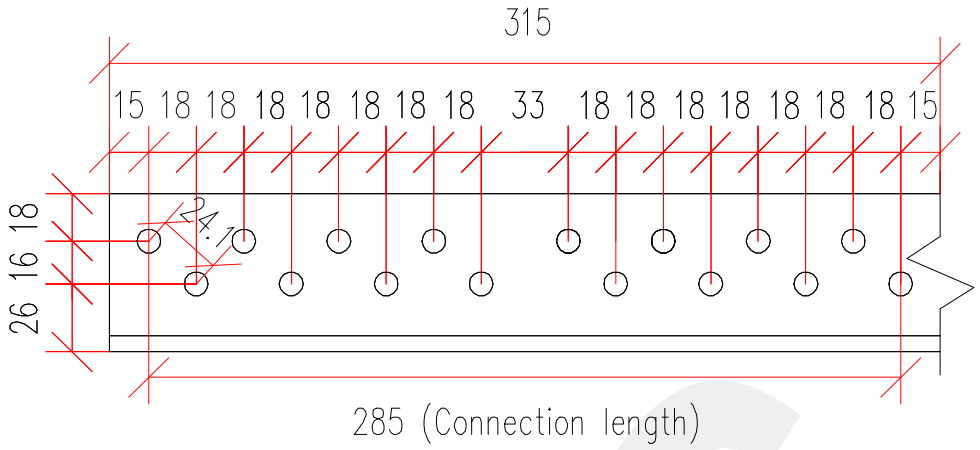

Figure A.1. Bolt distances (dimensions are in mm unit)

A.2. Gross Section Yielding Strength of Upper Main Member

Load level corresponding to yielding of gross cross section was calculated following the LRFD Method. The design expressions specified by the American Institute of Steel Construction AISC 360-10 Specifications were used as follows;

$P_n = F_y A_g$

P_n = 400 MPa x 6.91 cm^2

P_n =276.4 kN

Force in the upper main member, as specified by PLS-Tower program, was equal to 1317 kN

Scale $\rightarrow \frac{1317}{7.5}$ = 175.6 kN

276.4 kN > 175.6 kN √ O.K.

A.3. Net Section Fracture Strength of Upper Main Member

Fracture load capacity of net section is given as below;

$P_n = F_u A_e$

$A_e = U A_n$ (Effective Net Area) (1)

Shear lag factor is equal to 1.0 for the upper main member, because both legs of this member were connected to the lower main members.

U = 1.0 (LRFD Table D3.1) (2)

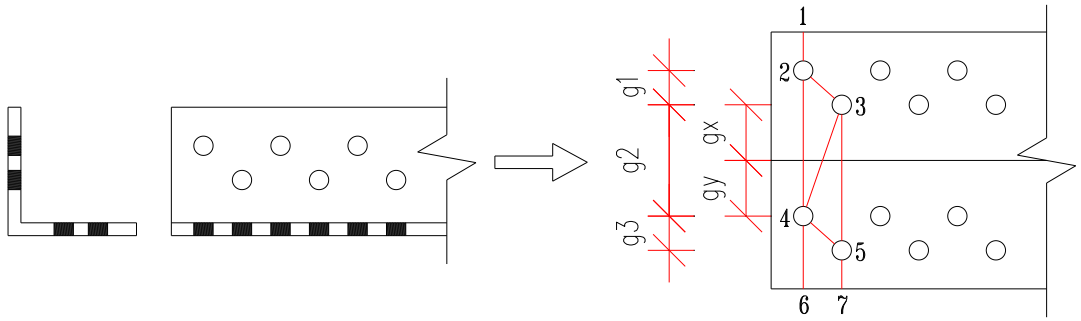

Figure A.2. Fracture paths considered in calculations

g1 = g3 = 16 mm

g2 = (gx + gy) – t = 26 + 26 - 6 = 46 mm

Path 1 (1-2-4-6)

A_{net}= 6.91 cm^2-(2×(0.80 cm+0.20 cm)×0.60 cm)= 5.71 cm^2

A_e = 1.0×5.71 cm^2= 5.71 cm^2

A_{req}= 0.85×A_g= 0.85×6.91cm^2= 5.87cm^2 → $A_e < A_{req}$ √ O.K.

P_n = 525 MPa×5.71 cm^2= 299.8 kN

Path 2 (1-2-3-4-6)

A_{net}=A_{gross}-(Lost area due to bolt holes)+(additional area due to staggered holes)

$$A_{net}=A_g-(3dt)+\left[\left(\frac{s^2}{4g}\right)\times t\right]$$

$$A_{net}= 6.91\ cm^2-\left(3\times(0.80\ cm+0.20\ cm)\times 0.60\ cm\right)+\left[\left(\frac{(1.80\ cm)^2}{4\times 1.60\ cm}\right)\times 0.60\ cm\right]$$

$$+\left[\left(\frac{(1.80\ cm)^2}{4\times 4.60\ cm}\right)\times 0.60\ cm\right] = 5.52\ cm^2$$

A_e= 1.0×5.52 cm^2= 5.52 cm^2

A_{req}= 0.85×A_g= 0.85×6.91cm^2= 5.87cm^2 → $A_e < A_{req}$ √ O.K.

P_n= 525 MPa×5.52 cm^2= 289.8 kN

Path 3 (1-2-3-4-5-7)

$$A_{net}= 6.91\ cm^2-(4\times(0.80\ cm+0.20\ cm)\times 0.60\ cm)+\left[\left(\frac{(1.80\ cm)^2}{4\times 1.60\ cm}\right)\times 0.60\ cm\right]$$

$$+\left[\left(\frac{(1.80\ cm)^2}{4\times 4.60\ cm}\right)\times 0.60\ cm\right]+\left[\left(\frac{(1.80\ cm)^2}{4\times 1.60\ cm}\right)\times 0.60\ cm\right]= 5.22\ cm^2$$

$A_e= 1.0\times 5.22\ cm^2= 5.22\ cm^2$

$A_{req}= 0.85\times A_g= 0.85\times 6.91 cm^2= 5.87 cm^2$ → $A_e < A_{req}$ √ O.K.

$P_n= 525\ MPa\times 5.22\ cm^2= 274.1\ kN$ (most critical)

Path 4 (1-2-3-5-7)

$$A_{net}= 6.91\ cm^2-(3\times(0.80\ cm+0.20\ cm)\times 0.60\ cm)+\left[\left(\frac{(1.80\ cm)^2}{4\times 1.60\ cm}\right)\times 0.60\ cm\right]= 5.41\ cm^2$$

$A_e= 1.0\times 5.41\ cm^2= 5.41\ cm^2$

$A_{req}= 0.85\times A_g=0.85\times 6.91 cm^2= 5.87 cm^2$ → $A_e < A_{req}$ √ O.K.

$P_n= 525\ MPa\times 5.41\ cm^2= 284\ kN$

P_n = 274.1 kN

Critical Path = Path 3 (1-2-3-4-5-7)

276.4 kN > 175.6 kN √ O.K.

A.4. Net Section Yielding Strength of Upper Main Member

Yielding strength of net section with most critical path is given as below;

$P_n = F_y A_e$

$$A_{net}= 6.91\ cm^2-(4\times(0.80\ cm+0.20\ cm)\times 0.60\ cm)+\left[\left(\frac{(1.80\ cm)^2}{4\times 1.60\ cm}\right)\times 0.60\ cm\right]$$

$$+\left[\left(\frac{(1.80\ cm)^2}{4\times 4.60\ cm}\right)\times 0.60\ cm\right]+\left[\left(\frac{(1.80\ cm)^2}{4\times 1.60\ cm}\right)\times 0.60\ cm\right]= 5.22\ cm^2$$

$A_e= 1.0\times 5.22\ cm^2= 5.22\ cm^2$

$A_{req}= 0.85\times A_g= 0.85\times 6.91 cm^2= 5.87 cm^2$ → $A_e < A_{req}$ √ O.K.

$P_n= 400\ MPa\times 5.22\ cm^2= 208.8\ kN$

It should be noted that net section yielding is not considered as a failure mode.

A.5. Bolt Shear Strength

The shear strength is given in Chapter J of LRFD as follows;

$P_n = F_{nv} A_b$ (3)

F_{nv} = shear stress from Table J3.2.

A_b = nominal unthreaded body area of bolt.

F_{nv} = 414 MPa

(Table J3.2, when threads are excluded from shear plane)

Connection has 32 M8 bolts,

$A_b = 32 \times 0.50\ cm^2 = 16\ cm^2$ (Area of one M8 bolt = 0.5 cm^2)

$P_n = 414\ MPa \times 16\ cm^2 = 662.4\ kN$ 662.4 kN >> 274.1 kN

Too many bolts were used.

$274.1\ kN = 414\ MPa \times A_b$ → $A_b = 6.62\ cm^2$

$N_{bolt} = \frac{6.62\ cm^2}{0.5\ cm^2} = 13.2$ → 14 M8 bolt is enough for connection.

A.6. Bearing Strength at Bolt Holes

The bearing strength at bolt holes was determined as follows;

$R_n = 1.2\ F_u\ L_e\ t \leq 2.4\ d\ t\ F_u$ (LRFD J3-6a) (4)

$1.2\ F_u L_e t = 1.2 \times 525\ MPa \times 1.50\ cm \times 0.60\ cm = 56.7\ kN$

$2.4\ d\ t\ F_u = 2.4 \times 0.80\ cm \times 0.60\ cm \times 525\ MPa = 60.5\ kN$

$R_n = 56.7\ kN < 60.5\ kN$

Bearing strength $R_n = 56.7\ kN$

A.7. Block Shear Strength

The strength corresponding to block shear rupture along a shear failure path and a perpendicular tension failure path was determined as follows;

$R_n = 0.6\ F_u\ A_{nv} + F_u\ A_{nt} \leq 0.6\ F_y\ A_{gv} + F_u\ A_{nt}$ (LRFD J4-5) (5)

A_{gv} = gross area subject to shear

A_{nt} = net area subject to tension

A_{nv} = net area subject to shear

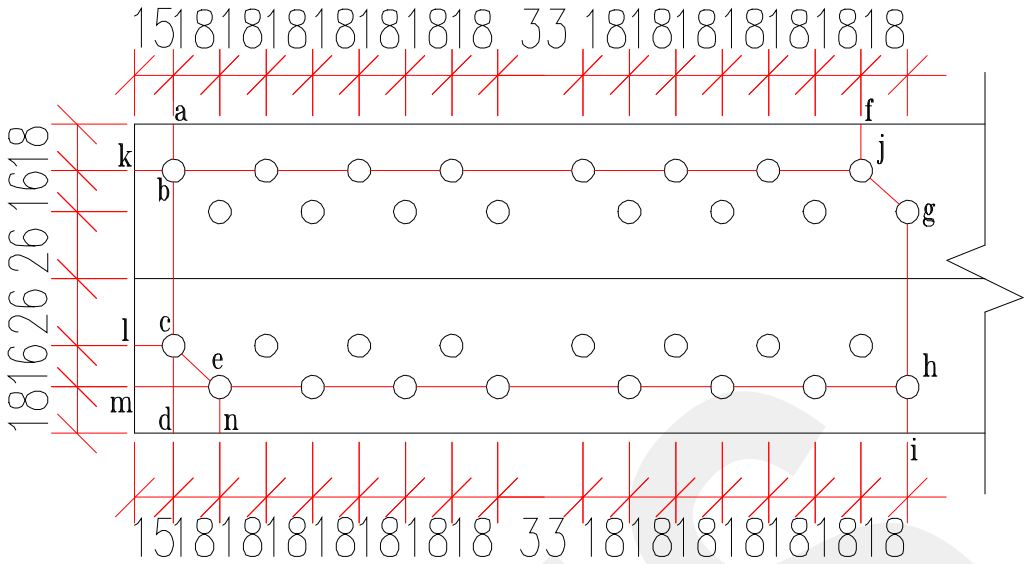

Figure A.3. Block shear paths (all dimensions are in mm unit)

Path 1 (k-b-j-g-h-i)

A_{gv}= (28.20 cm×0.60 cm)+(cos45×2.41 cm×0.60 cm)= 17.94 cm^2

A_{nv}= 17.94 cm^2-(8.5×(1.00 cm×0.60 cm))= 12.84 cm^2

A_{nt}= (8.60 cm×0.60 cm)+(cos45×2.41 cm×0.60 cm)-(2.5×(1.00 cm×0.60cm))= 4.68 cm^2

R_{n1}= 0.6×525 MPa×12.84 cm^2 +525 MPa×4.68 cm^2= 650.2 kN (Most critical)

R_{n2}= 0.6×400 MPa×17.94 cm^2 +525 MPa×4.68 cm^2= 676.3 kN

R_n = 650.2 kN

Path 2 (l-c-e-h-g-j-f)

A_{gv}= (28.20 cm×0.60 cm)+2×(cos45×2.41 cm×0.60 cm)= 18.96 cm^2

A_{nv}= 18.96 cm^2-(8.5×(1.00 cm×0.60 cm))= 13.86 cm^2

A_{nt}= (8.60 cm×0.60 cm)+2×(cos45×2.41 cm×0.60 cm)-(2.5×(1.00 cm×0.60cm))= 5.70 cm^2

R_{n1}= 0.6×525 MPa×13.86 cm^2 +525 MPa×5.70 cm^2= 735.8 kN

R_{n2}= 0.6×400 MPa×18.96 cm^2 +525 MPa×5.70 cm^2= 754.3 kN

R_n = 735.8 kN

Path 3 (k-b-j-g-h-e-m)

A_{gv}= (28.20 cm×0.60 cm)+(cos45×2.41 cm×0.60 cm)+(30.00 cm×0.60 cm) = 35.94 cm^2

A_{nv}= 35.94 cm^2-(16×(1.00 cm×0.60 cm))= 26.34 cm^2

A_{nt}= (8.60 cm×0.60 cm)+(cos45×2.41 cm×0.60 cm)-$\left(2.5\times(1.00\ cm\times 0.60cm)\right)$= 4.68 cm^2

R_{n1}= 0.6×525 MPa×26.34 cm^2 +525 MPa×4.68 cm^2= 1075.4 kN

R_{n2}= 0.6×400 MPa×35.94 cm^2 +525 MPa×4.68 cm^2= 1108.3 kN

R_n = 1075.4 kN

Path 4 (k-b-j-g-h-e-c-l)

A_{gv}= 2×(28.20 cm×0.60 cm)+2×(cos45×2.41 cm×0.60 cm)= 35.88 cm^2

A_{nv}= 35.88 cm^2-(17×(1.00 cm×0.60 cm))= 25.68 cm^2

A_{nt}= (6.80 cm×0.60 cm)+2×(cos45×2.41 cm×0.60 cm)-$\left(3.5\times(1.00\ cm\times 0.60cm)\right)$= 4.02 cm^2

R_{n1}= 0.6×525 MPa×25.68 cm^2 +525 MPa×4.02 cm^2= 1020 kN

R_{n2}= 0.6×400 MPa×35.88 cm^2 +525 MPa×4.68 cm^2= 1106.8 kN

R_n = 1020 kN

Path 5 (a-b-j-g-h-e-n)

A_{gv}= 2×(26.70 cm×0.60 cm)+(cos45×2.41 cm×0.60 cm) = 33.06 cm^2

A_{nv}= 33.06 cm^2-(15×(1.00 cm×0.60 cm))= 24.06 cm^2

A_{nt}= 2×(1.8 cm×0.6 cm)+(6.80 cm×0.60 cm)+(cos45×2.41 cm×0.60 cm)
-$\left(3\times(1.00\ cm\times 0.60cm)\right)$= 5.46 cm^2

R_{n1}= 0.6×525 MPa×24.06 cm^2 +525 MPa×5.46 cm^2= 1044.5 kN

R_{n2}= 0.6×400 MPa×25.68 cm^2 +525 MPa×5.46 cm^2= 903 kN

R_n = 903 kN

Block shear strength R_n = 650.2 kN

Critical Path : Path 1 (k-b-j-g-h-i)

A.8. Summary of Design Considerations

The above calculations indicate that the load capacity is 274.1 kN, and the failure mode is net section fracture. The critical fracture path is Path 3 (1-2-3-4-5-7).